Received: 14 October 2022 | Revised: 5 May 2023 | Accepted: 11 June 2023

IET Generation, Transmission & Distribution

DOI: 10.1049/gtd2.12915

The Institution of Engineering and Technology WILEY

ORIGINAL RESEARCH

Coordinated planning of charging swapping stations and active distribution network based on EV spatial-temporal load forecasting

Chenke He[1] | Jizhong Zhu[1] | Alberto Borghetti[2] | Yun Liu[1] | Shenglin Li[1]

[1]School of Electric Power Engineering, South China University of Technology, Guangzhou, China

[2]Department of Electrical, Electronic and Information Engineering, University of Bologna, Bologna, Italy

Correspondence
Jizhong Zhu and Shenglin Li, School of Electric Power Engineering, South China University of Technology, Guangzhou, China.
Email: zhujz@scut.edu.cn; eplishl@mail.scut.edu.cn

Funding information
National Natural Science Foundation of China, Grant/Award Number: 52177087; High-end Foreign Experts Project, Grant/Award Number: G2022163018L; Science and Technology Projects in Guangzhou, Grant/Award Number: 202201010354

Abstract

Electric vehicles (EVs) charging swapping stations (CSSs), as well as multi-functional integrated charging and swapping facilities (CSFs), have become important to reduce the impact of e-mobility on the electric power distribution system. This paper presents a coordinated planning optimization strategy for CSSs/CSFs and active distribution networks (AND) that includes distributed generation. The approach is based on the application of a specifically developed spatial-temporal load forecasting method of both plug-in EVs (PEVs) and swapping EVs (SEVs). The approach is formulated as a mathematical programming optimization model that provides the location and sizing of new CSSs, the best active distribution network topology, the required distributed generation, and substation capacities. The developed model is solved using CPLEX, and its characteristics and performances are evaluated through a realistic case study.

1 | INTRODUCTION

In recent years, growing concerns on environmental pollution issues cause a steady increase in the penetration of electric vehicles (EVs) in active distribution networks (ADNs). The power requirements due to the use of EVs has strong spatial-temporal uncertainty, which proposes a new challenge to the planning of ADNs. This paper focuses on charging and swapping stations (CSS), also called charging and swapping facilities (CSF), composed by both a charging system (CS) and a swapping and charging system (SCS), able to satisfy the load demand of plug-in EVs (PEVs) and swapping EVs (SEVs) simultaneously.

Accurate forecasting of EV load is the premise of optimal planning of CSSs. The literature on the subject mostly focuses on the PEV load forecasting [1–22]. Some approaches aim at providing the medium-long-term forecasting of EV load, for example, the overall load change of PEVs in different years [1–4]. Deep learning method are used to obtain PEV load curves [5–12]. Some approaches propose a forecast of the PEV load curves based on the EVs travel chains analysis [13] or queuing theory [14]. Spatial-temporal EV load forecasting is also documented, which can provide the curves of PEV loads [16–18, 20–22] or a fixed PEV load spatial distribution [15, 19]. Locating and sizing new CSSs needs both the EV load curves and the EV load spatial distribution.

SEV load forecasting is dealt with different approaches: PEV data are used to forecast the SEV load or to obtain the load curve of SEVs [23, 25–29] or fixed SEV load spatial distributions are assumed [24].

Differently from the typical long charging duration of PEV (from half an hour to several hours), the swapping process of SEV is completed in a few minutes [23]. The traditional PEV load forecasting method is no longer applicable to predict the load of SEVs and a new specifically developed approach is needed.

Currently, studies on stations with a single function (charging or swapping) are relatively well documented (e.g. [30–32] for charging station and [24, 33] for swapping station). To satisfy the requests associated with the use of PEVs and SEVs (i.e. different types EV loads) in a region, it is usually necessary to build

various types of stations [34–37], which may involve multiple investment stakeholders. Therefore, it is difficult to unify the planning and the coordinated operation with the ones of ADNs. The CSS is a new type of EV multi-functional centralized station, which combines the charging system and swapping system in one station. CSS can reduce EV load fluctuations through the complementary operation of CS and SCS.

Within this context, the integrated planning should appropriately consider the coupling between CSFs and ADN. Whilst in [34, 35, 38–42] new charging stations are planned in a fixed ADN configuration, a better coordination of the charging station planning with the one of distributed generation (DG) and ADN is proposed in [43–49]. In addition, several comprehensive planning methods for CSFs adopt the load forecasting for PEVs explicitly [50, 51].

The above-mentioned papers show the advantages of coordinated planning that can improve power supply reliability, power quality, EV adoption, operation efficiency, as well as reduce planning investment and waste. Furthermore, inadequate coordination between the planning and operation of charging stations and ADN could impede the construction of additional charging stations and may require large capacity energy storage systems to prevent vulnerabilities.

In addition, with the process of rapid improvement of smart grid technology and electric transportation systems, the network may experience the negative effects of cyberattacks [52], such as congestions, power shortages, and other technical issues [53]. Power outages due to cyberattacks are documented in [54, 55]. While the paper is not focused on cybersecurity, the following considerations could serve as a preliminary introduction. Detailed information on the power system configurations, electrified transportation systems, and applied smart grids technologies favour successful cyberattacks [53, 56, 57]. Therefore, the planning and operational data of most utilities are not publicly available. Distribution system operators can take advantage of EVs as mobile energy storage units to mitigate the impact of cyberattacks. For example, they can use CSFs as emergency power supplies to alleviate the consequences of false information injection, by providing support to the affected load nodes, reducing overload disconnections of power lines, and facilitating fault recovery. In addition, the development of CSFs, which provides the control of charging operations for a large number of EVs and for energy storage swapping, could overcome the challenge of coordinating dispersed low-power EV charging devices (e.g. household EV chargers) through the use of aggregators, local electricity markets, and demand response techniques [53].

This paper presents a coordinated planning approach of CSS and ADN. The approach involves the development of an EV spatial-temporal load forecasting method for PEVs and SEVs, followed by the construction of a configuration model of CSS and ADN. Using these models, the coordinated planning model is obtained, the effectiveness of which is validated through case studies.

The main contributions are summarized as follows.

1. An EV spatial-temporal load forecasting method is developed. This method includes the analysis of the temporal and spatial characteristics of EV's travel patterns, considering the type of region, the departure time, the driving duration, and parking time. Driving carbon emissions are used to guide EVs for charging and swapping. Coupling EV charging and swapping processes with driving and parking processes provides the forecasting of EV spatial-temporal load, considering EV load distribution, CSS layout, planning area roads, and other factors.
2. The configuration models of CSS and ADN are developed. The configuration models of CS and SCS are obtained from their operation, service, and structure characteristics. The analysis of the coupling between CS and SCS in terms of planning and operation provides the configuration model of CSS, considering its multifunctional and integrated characteristics. The configuration model of ADN network includes the analysis of DG penetration.
3. A coordinated planning model of CSS and ADN is developed, considering the EV spatial-temporal load forecasting. The aim is to minimize the annual planning comprehensive cost considering location and size of CSSs, the ADN configuration, the size of substations and DGs, as well as the carbon emission of EVs.

The rest of this paper is organized as follows. Section 2 describes the EV spatial-temporal load forecasting method. Section 3 is devoted to the configuration models of CSS and ADN. Section 4 presents the coordinated planning method. Section 5 illustrates the analysis of the case studies. Section 6 provides the conclusions.

2 | EV SPATIAL-TEMPORAL LOAD FORECASTING METHOD

The travel patterns of EV are analysed from the temporal and spatial aspects. The EV driving carbon emissions are used to guide them to the charging stations. The flow chart of the EV spatial-temporal load forecasting method is shown in Figure 1.

2.1 | Analysis of EV travel chains

2.1.1 | The temporal characteristics analysis of travels

National household travel survey (NHTS) data is used to model the EVs charging demand [9, 58, 59]. The EV daily initial departure time is represented by the gamma distribution (1). The EV parking durations in the working regions (WRs) and commercial regions (CRs) can be represented by the generalized extreme value distributions (2) and (3), respectively. The driving process of EV is divided into three types:

a. Type I—EVs drive from a residential region (RR) to a non-RR (e.g. WR, CR);
b. Type II—EVs drive from a non-RR to a non-RR;
c. Type III—EVs drive from a non-RR to a RR.

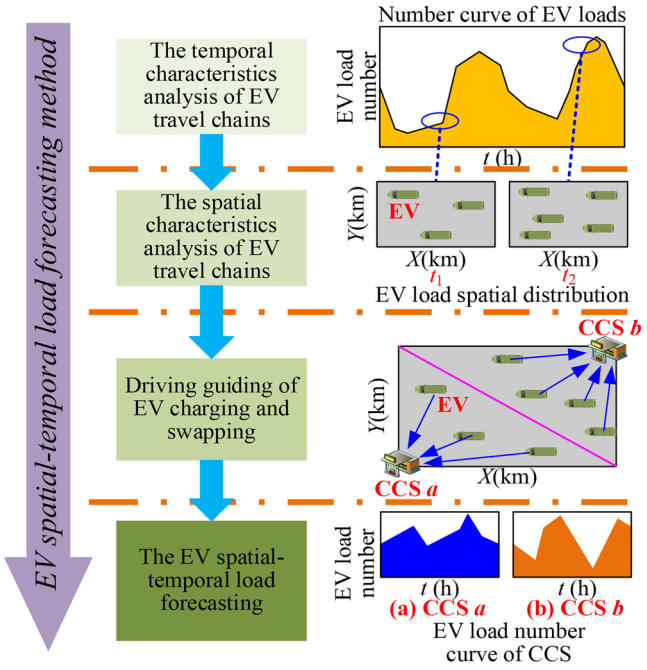

FIGURE 1 The overall flow chart of EV spatial-temporal load forecasting method.

The duration of the above three types of driving processes follows lognormal distributions (4).

$$f(t_{\mathrm{L}}) = \frac{58.908^{9.881}}{\Gamma(9.881)} t_{\mathrm{L}}^{9.881-1} e^{-58.908 t_{\mathrm{L}}} \tag{1}$$

$$\begin{cases} z = \dfrac{t_{\mathrm{P}} - 438.445}{164.506} \\ f(z) = \dfrac{1}{164.506} e^{-(1-0.234z)^{-1/(-0.234)}} \times (1-0.234z)^{-1-1/(-0.234)} \end{cases} \tag{2}$$

$$\begin{cases} z = \dfrac{t_{\mathrm{P}} - 68.520}{41.761} \\ f(z) = \dfrac{1}{41.761} e^{-(1+0.657z)^{-1/0.657}} \times (1+0.657z)^{-1-1/0.657} \end{cases} \tag{3}$$

$$\begin{cases} f(t_{\mathrm{D}}) = \dfrac{1}{t_{\mathrm{D}}\sigma\sqrt{2\pi}} e^{-[\ln(t_{\mathrm{D}})-\mu]^2/(2\sigma^2)} \\ (1)\ \text{TypeI}: \begin{cases} \mu = 3.020 \\ \sigma = 0.775 \end{cases}; \ \text{Type(2) II}: \begin{cases} \mu = 2.846 \\ \sigma = 0.815 \end{cases}; \\ (3)\ \text{TypeIII}: \begin{cases} \mu = 3.040 \\ \sigma = 0.761 \end{cases} \end{cases} \tag{4}$$

where t_{L} is the EV initial departure time. Δt_{P} is the EV parking duration in a certain region (e.g. WR and CR). z is an intermediate variable. Δt_{D} is the EV driving duration between two certain regions. μ and σ are the probability density function parameters of EV driving duration.

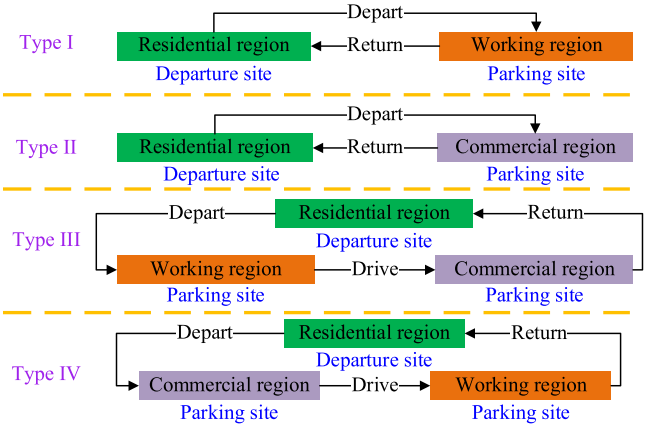

FIGURE 2 The EV typical travel chains.

2.1.2 | The spatial characteristics analysis of travels

The charging and swapping load demand of EVs depend on the driving distance between the arrival and departure sites and the remaining battery level. There is a strong coupling between EV load demands (i.e. charging and swapping processes) and travel demands (i.e. driving and parking processes). The departure sites, parking sites, and destinations of EVs travel chains can be classified into WRs, CRs, and RRs. Commonly, a daily trip of EV starts from an RR and finally returns to the same RR. The purpose of daily trip is often for work or entertainment. The EV travel chains are divided into four typical types, illustrated in Figure 2:

a. Type I—EV departs from the RR to the WR in the morning (i.e. parking a period of time, and mainly to work etc.) and return to the RR later;
b. Type II—EV departs from the RR to the CR in the morning (i.e. parking a period of time, and mainly to entertain etc.) and return to the RR later;
c. Type III—EV departs from the RR to the WR in the morning, and then driving from the WR to the CR, and return to the RR later;
d. Type IV—EV departs from the RR to the CR in the morning, and then driving from the CR to the WR, and return to the RR later.

2.2 | Driving guide to charging and swapping

To fully consider the environmental protection factors of EV charging statin planning, the driving carbon emissions between the EV load demand site to the charging station are used. The EVs' daily total carbon emission E_{CO2} for charging and swapping in the planning area is represented by (5).

$$E_{\mathrm{CO2}} = \beta_{\mathrm{CO2}} \sum_{t=1}^{T} \sum_{i=1}^{N_{\mathrm{CSS}}} \left(e_{\mathrm{PEV}} \sum_{j=1}^{N_{i,t}^{\mathrm{PEV}}} D_{i,j,t}^{\mathrm{PEV,min}} + e_{\mathrm{SEV}} \sum_{k=1}^{N_{i,t}^{\mathrm{SEV}}} D_{i,k,t}^{\mathrm{SEV,min}} \right) \tag{5}$$

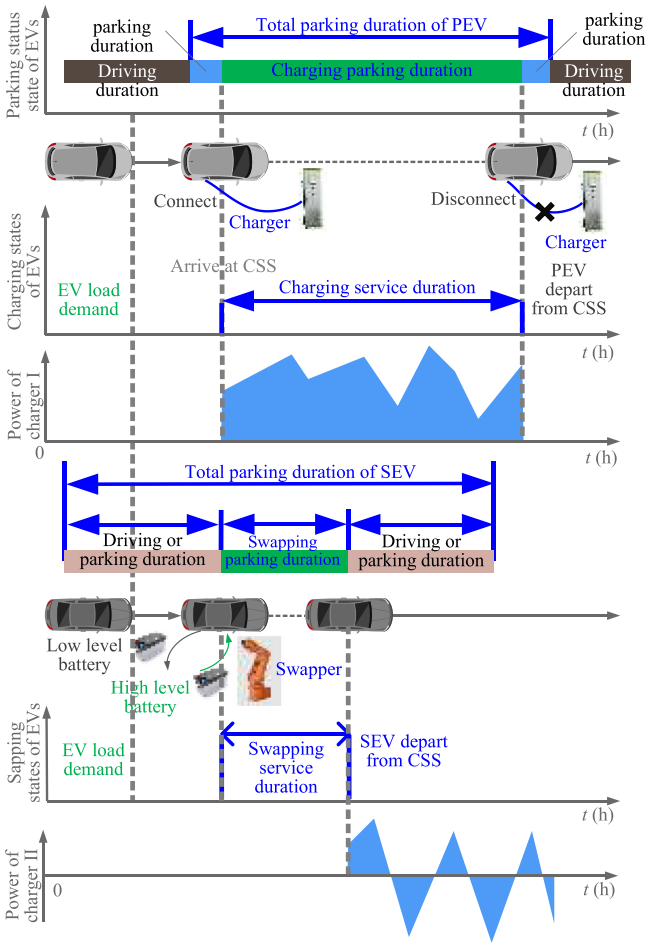

FIGURE 3 The coupling between EV charging and swapping processes with driving and parking processes.

where β_{CO2} is the carbon emissions per unit of electric energy of traditional generating units; T is the total hour per day [33]; N_{CSS} is the number of CSSs; $N_{i,t}^{PEV}$ and $N_{i,t}^{SEV}$ are the load numbers of PEVs and SEVs of CSS i at time t, respectively; e_{PEV} and e_{SEV} are the energy consumption per unit driving distance of a PEV and a SEV, respectively; $D_{i,j,t}^{PEV,min}$ and $D_{i,k,t}^{SEV,min}$ are the minimum driving distances of PEV j and SEV k that drive to CSS I, respectively.

2.3 | The EV spatial-temporal load forecasting

Figure 3 illustrates the integration of EV charging and swapping processes with the driving and parking processes. Due to the significant charging duration of a PEV, it is impractical to charge the PEV during the travel (the extreme scenario of completely depleting the battery charge is not considered). Thus, the charging of PEVs typically occurs during parking periods. Simultaneously, to ensure that the battery level can meet the driving demand at the end of the parking period, the PEV is generally charged immediately when parked. Conversely, the

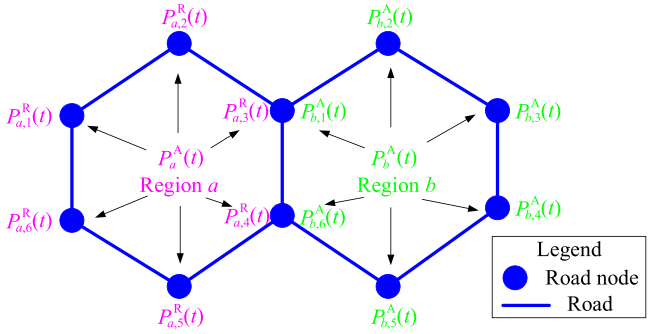

FIGURE 4 The EV load probabilities relationship between the region and road nodes.

SEVs can swap batteries both during the travel or initial parking (i.e. a SEV generally does not go to a charging station for a battery swap after the initial parking).

Based on the above assumptions, the two steps of the proposed EV spatial-temporal load forecasting method are:

Step 1—simulation of travel chains, charging, and swapping demands of EVs.

Firstly, regions (i.e. RR, CR, and WR) and road nodes in the planning area are numbered. The roulette method [37] is adopted to simulate the travel chain types of EVs, as well as the region numbers where EVs are located at different times. The duration of parking and driving processes of EVs are represented by (6). The EV battery level $E_i^{EV,S}$ that accomplish the driving process I is represented by (7). If the $E_i^{EV,S}$ is lower than the minimum battery level [60], the EV will request a load demand for charging and swapping. Thus, the PEV initial charging time t_C^{PEV} meets (8), and the SEV swapping time t_S^{SEV} satisfies (9). The probability of an EV requesting a charge demand in a specific region is represented by (10). Based on this, the probability matrix of EVs charging demands at road nodes is constructed, according to (11). The relationship among region i EV load probability and the EV load probabilities of road nodes in region i is represented by (12). Specifically, the EV load probabilities of road nodes are calculated by the roulette method [37] based on the region i EV load probability. Then, based on the travel chain types of EVs, the Monte Carlo method [44] is used to sample the specific travel chain information.

$$t_i^P = t_L + \sum_{\forall i} (\Delta t_i^P + \Delta t_i^D) \tag{6}$$

$$E_i^{EV,S} = E_{i-1}^{EV,S} - e_{EV} V_{i-1}^{EV,D} \Delta t_{i-1}^D, \forall i, EV \in \{PEV, SEV\} \tag{7}$$

$$\begin{cases} t_C^{PEV} = t_{i-1}^P, E_i^{PEV,S} \le SOC_{min} E_{max}^{PEV} \\ t_C^{PEV} = [], \text{others(PEVdoesnotcharge)} \end{cases}, \forall i \tag{8}$$

$$\begin{cases} t_{\mathrm{S}}^{\mathrm{SEV}} = t_{\mathrm{S,a}}^{\mathrm{SEV}}, \\ \begin{cases} t_{\mathrm{S,a}}^{\mathrm{SEV}} \sim U\left(t_{\mathrm{L}} + \sum_{\forall i}\left[\Delta t_{i-1}^{\mathrm{P}} + \Delta t_{i}^{\mathrm{D}}\right], t_{\mathrm{L}} + \sum_{\forall i}\left[\Delta t_{i}^{\mathrm{P}} + \Delta t_{i}^{\mathrm{D}}\right]\right) \\ E_{i}^{\mathrm{SEV,S}} \le SOC_{\min} E_{\max}^{\mathrm{SEV}} \end{cases}, \forall i \\ t_{\mathrm{S}}^{\mathrm{SEV}} = t_{\mathrm{S,b}}^{\mathrm{SEV}}, t_{\mathrm{S,b}}^{\mathrm{SEV}} = t_{i}^{\mathrm{P}}, E_{i}^{\mathrm{SEV,S}} \le SOC_{\min} E_{\max}^{\mathrm{SEV}} \\ t_{\mathrm{S}}^{\mathrm{SEV}} = [], \text{others(SEVdoesnotswapbatteries)} \end{cases} \quad (9)$$

$$\mathbf{P}_{t}^{\mathrm{a}} = \left[P_{1,t}^{\mathrm{a}}, P_{2,t}^{\mathrm{a}}, P_{3,t}^{\mathrm{a}}, \ldots, P_{N_{\mathrm{a}},t}^{\mathrm{a}}\right], \sum_{i=1}^{N_{\mathrm{a}}} P_{i,t}^{\mathrm{a}} = 1, \forall t \quad (10)$$

$$P_{t}^{r} = \begin{bmatrix} P_{1,1,t}^{r} & P_{1,2,t}^{r} & \cdots & P_{1,N_r,t}^{r} \\ P_{2,1,t}^{r} & P_{2,2,t}^{r} & \cdots & P_{2,N_r,t}^{r} \\ \vdots & \vdots & \ddots & \vdots \\ P_{N_a,1,t}^{r} & P_{N_a,2,t}^{r} & \cdots & P_{N_a,N_r,t}^{r} \end{bmatrix} \quad (11)$$

$$P_{i,t}^{\mathrm{a}} = \sum_{j \in \mathfrak{V}_i} P_{i,j,t}^{\mathrm{r}}, \forall i, \forall t \quad (12)$$

In (6)–(12) t_{P} is the initial parking time that EV just arrived at a region; Δt_i^P and Δt_i^D are the parking duration i and driving duration i of an EV, respectively; $V_{i-1}^{\mathrm{EV,D}}$ is the EV average driving speed of driving process i; $E_{\max}^{\mathrm{PEV}}$ is the energy storage (ES) capacity of a PEV; $t_{\mathrm{S,a}}^{\mathrm{SEV}}$ and $t_{\mathrm{S,b}}^{\mathrm{SEV}}$ are the SEV possible swapping time a and b, respectively; $E_{\max}^{\mathrm{SEV}}$ is the ES capacity of a SEV; $\mathbf{P}_t^a$ and $\mathbf{P}_t^r$ are the EVs load demand probabilities matrixes of regions and road nodes at time t, respectively; $P_{i,t}^a$ and $P_{i,j,t}^r$ are the EVs load demand probabilities in region i and in road node j (belonging to region i) at time t, respectively; $\mathfrak{V}_i$ is the set of road nodes that belong to region i; N_{a} and N_{r} are the numbers of regions and road nodes in the planning area respectively.

The EV load probabilities relationship between region and road nodes are shown in Figure 4. EV driving and parking processes with different types of travel chains are illustrated in Figure 5.

Step 2—Multi scenarios forecasting and scenarios clustering.

By repeating the step 1 above, $T \times N_{\mathrm{SC}}$ EV load distribution scenarios are obtained (T are the coordinates of EVs that request charging and swapping according to (13) and N_{SC} is the number of scenarios simulated at the same time slot). The K-means clustering method [24] is used to obtain a reduced set of typical scenarios, according to (14). EV load number set $\mathbf{N}_t^r$ for all road nodes at time t is obtained by using (15). EV load mapping matrix $\mathbf{N}_t^{\mathrm{r,C}}$ between road nodes and CSSs at time t is constructed through (16). EV load number set $\mathbf{N}_t^C$ for all CSSs at time t is calculated by using (17).

$$\begin{cases} \mathbf{W}_{t,i}^{\mathrm{EV}} = \left[\mathbf{w}_{t,i}^{\mathrm{EV}}(1), \mathbf{w}_{t,i}^{\mathrm{EV}}(2), \ldots, \mathbf{w}_{t,i}^{\mathrm{EV}}(N_{t,i}^{\mathrm{EV}})\right] \\ \mathbf{CO}_{t,i,j}^{\mathrm{EV}} = (X_{t,i,j}^{\mathrm{EV}}, Y_{t,i,j}^{\mathrm{EV}}) \end{cases}, \quad \begin{cases} \mathrm{EV} \in \{\mathrm{PEV}, \mathrm{SEV}\} \\ \forall t \end{cases} \quad (13)$$

$$\overbrace{\begin{bmatrix} W_{1,1}^{\mathrm{EV}} & W_{1,2}^{\mathrm{EV}} & \ldots & W_{1,N_{\mathrm{SC}}}^{\mathrm{EV}} \\ W_{2,1}^{\mathrm{EV}} & W_{2,2}^{\mathrm{EV}} & \ldots & W_{2,N_{\mathrm{SC}}}^{\mathrm{EV}} \\ \vdots & \vdots & \ddots & \vdots \\ W_{T,1}^{\mathrm{EV}} & W_{T,2}^{\mathrm{EV}} & \ldots & W_{T,N_{\mathrm{SC}}}^{\mathrm{EV}} \end{bmatrix}}^{SW_{\mathrm{To}}^{\mathrm{EV}}} \xrightarrow{\text{Clustering}} \overbrace{\begin{bmatrix} W_{\mathrm{EV}}(1) \\ W_{\mathrm{EV}}(2) \\ \vdots \\ W_{\mathrm{EV}}(T) \end{bmatrix}}^{SW_{\mathrm{Ty}}^{\mathrm{EV}}} \xrightarrow{\text{Mapping}}$$

$$\overbrace{\begin{bmatrix} W_{1,1}^{\mathrm{EV,R}} & W_{1,2}^{\mathrm{EV,R}} & \ldots & W_{1,T}^{\mathrm{EV,R}} \\ W_{2,1}^{\mathrm{EV,R}} & W_{2,2}^{\mathrm{EV,R}} & \ldots & W_{2,T}^{\mathrm{EV,R}} \\ \vdots & \vdots & \ddots & \vdots \\ W_{N_R,1}^{\mathrm{EV,R}} & W_{N_R,2}^{\mathrm{EV,R}} & \ldots & W_{N_R,T}^{\mathrm{EV,R}} \end{bmatrix}}^{SW_{R}^{\mathrm{EV}}} \xrightarrow{\text{Guided driving}} \overbrace{\begin{bmatrix} N_{r,1,t}^{\mathrm{EV}} \\ N_{r,2,t}^{\mathrm{EV}} \\ \vdots \\ N_{r,N_R,t}^{\mathrm{EV}} \end{bmatrix}}^{N_t^r}$$

$$W_{j,t}^{\mathrm{EV,R}} = \left[w_{t,j}^{\mathrm{EV,R}}(1), w_{t,j}^{\mathrm{EV,R}}(2), \ldots, w_{t,j}^{\mathrm{EV,R}}\left(N_{t,j}^{\mathrm{EV,R}}\right)\right], \quad \mathrm{EV} \in \{\mathrm{PEV}, \mathrm{SEV}\}, \forall t \quad (14)$$

$$\overbrace{\begin{bmatrix} N_{r,1,t}^{\mathrm{EV}} \\ N_{r,2,t}^{\mathrm{EV}} \\ \vdots \\ N_{r,N_r,t}^{\mathrm{EV}} \end{bmatrix}}^{N_t^r} \xrightarrow{\text{Mapping}} \overbrace{\begin{bmatrix} N_{1,1,t}^{\mathrm{EV}} & N_{1,2,t}^{\mathrm{EV}} & \cdots & N_{1,N_r,t}^{\mathrm{EV}} \\ N_{2,1,t}^{\mathrm{EV}} & N_{2,2,t}^{\mathrm{EV}} & \cdots & N_{2,N_r,t}^{\mathrm{EV}} \\ \vdots & \vdots & \ddots & \vdots \\ N_{N_C,1,t}^{\mathrm{EV}} & N_{N_C,2,t}^{\mathrm{EV}} & \cdots & N_{N_C,N_r,t}^{\mathrm{EV}} \end{bmatrix}}^{N_t^{\mathrm{r,C}}}$$

$$\xrightarrow{\text{Mapping}} \overbrace{\begin{bmatrix} N_{1,t}^{\mathrm{EV}} \\ N_{2,t}^{\mathrm{EV}} \\ \vdots \\ N_{N_C,t}^{\mathrm{EV}} \end{bmatrix}}^{N_t^C}, \quad \mathrm{EV} \in \{\mathrm{PEV}, \mathrm{SEV}\}, \forall t \quad (15)$$

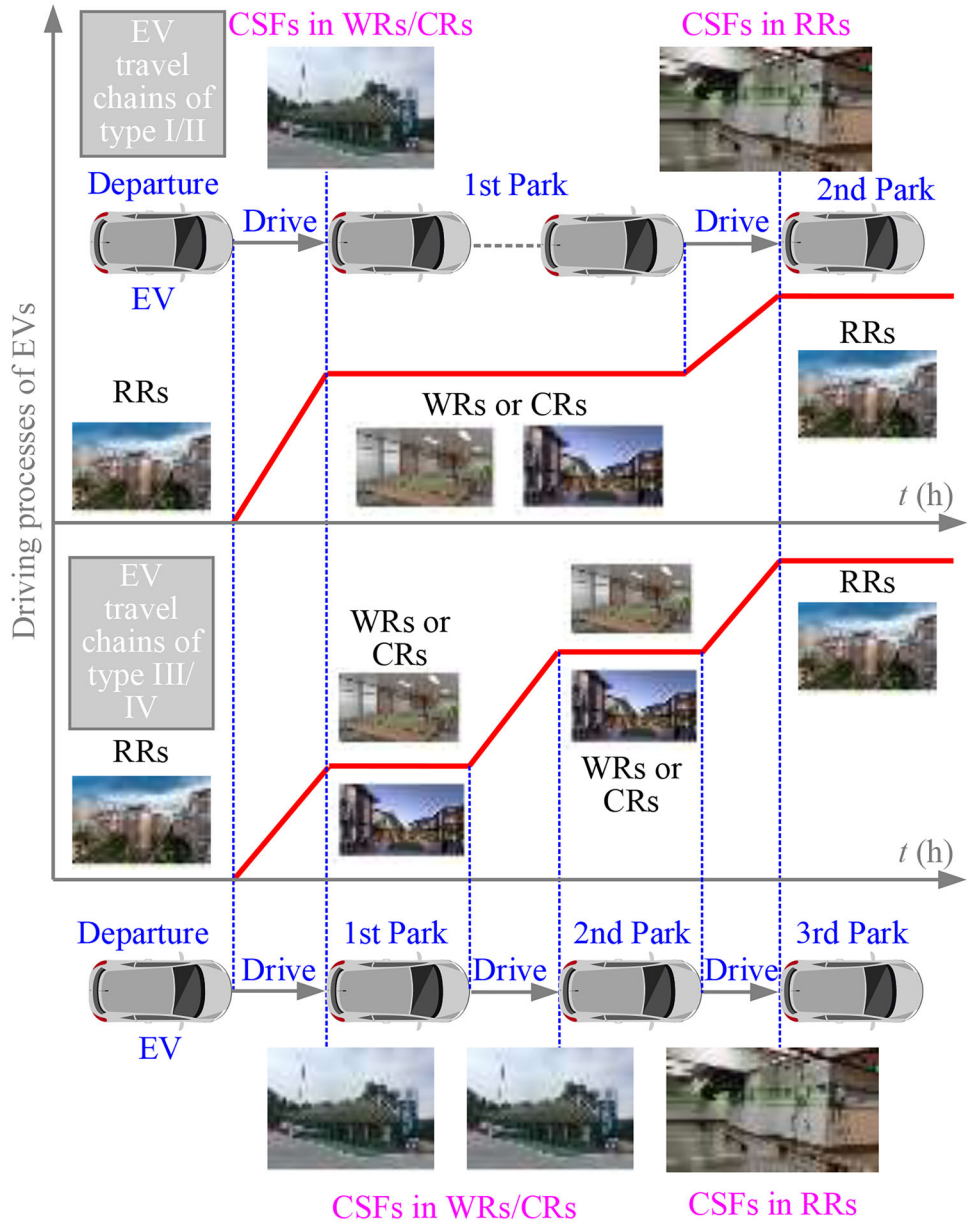

FIGURE 5 The EV driving and parking processes with different types of travel chains.

$$\begin{cases} N_{j,k,t}^{\mathrm{EV}} = \begin{cases} N_{\mathrm{R},k,t}^{\mathrm{EV}}, \min\left\{L_{j,k}^{\mathrm{R}}\right\} \\ , (\text{Closest between road node } k \text{ and CSS } j) \\ 0, \text{Others} \end{cases} \\ N_{j,k,t}^{\mathrm{EV}} \in \mathbf{N}_t^{\mathrm{r,C}}, N_{\mathrm{R},k,t}^{\mathrm{EV}} \in \mathbf{N}_t^{\mathrm{r}}, \mathrm{EV} \in \{\mathrm{PEV}, \mathrm{SEV}\}, \forall j, \forall k, \forall t \end{cases} \tag{16}$$

$$\begin{cases} N_{j,t}^{\mathrm{EV}} = \sum_{\forall k} N_{j,k,t}^{\mathrm{EV}}, N_{j,t}^{\mathrm{EV}} \in \mathbf{N}_t^{\mathrm{C}}, N_{j,k,t}^{\mathrm{EV}} \in \mathbf{N}_t^{\mathrm{r,C}}, \\ \mathrm{EV} \in \{\mathrm{PEV}, \mathrm{SEV}\}, \forall j, \forall k, \forall t \end{cases} \tag{17}$$

In (13)–(17) $\mathbf{W}_{t,i}^{\mathrm{EV}}$ is the EV spatial-temporal load scenario i at time t; $\mathbf{CO}_{t,i}^{\mathrm{EV}}(j)$ and $(X_{t,i}^{\mathrm{EV}}(j), Y_{t,i}^{\mathrm{EV}}(j))$ are the load coordinates of EV j at time t; $\mathbf{SW}_{\mathrm{To}}^{\mathrm{EV}}$ and $\mathbf{SW}_{\mathrm{Ty}}^{\mathrm{EV}}$ are the total and typical scenarios of EV load distribution, respectively; $\mathbf{SW}_{R}^{\mathrm{EV}}$ is the mapping matrix between EV load coordinates and road nodes; $\mathbf{W}_{j,t}^{\mathrm{EV,R}}$ is the EV load coordinates that belong to road node j at time t; $\mathbf{CO}_{t,i,j}^{\mathrm{EV}}$ is the EV load coordinate i that belong to road node j at time t; $N_{t,j}^{\mathrm{EV,R}}$ is the number of EV load coordinates that belong to road node j at time t; $N_{R,k,t}^{\mathrm{EV}}$ is the EVs load number at road node k and time t; $N_{j,k,t}^{\mathrm{EV}}$ is the EV load number mapping between road node k and CSS j at time t; $N_{j,t}^{\mathrm{EV}}$ is

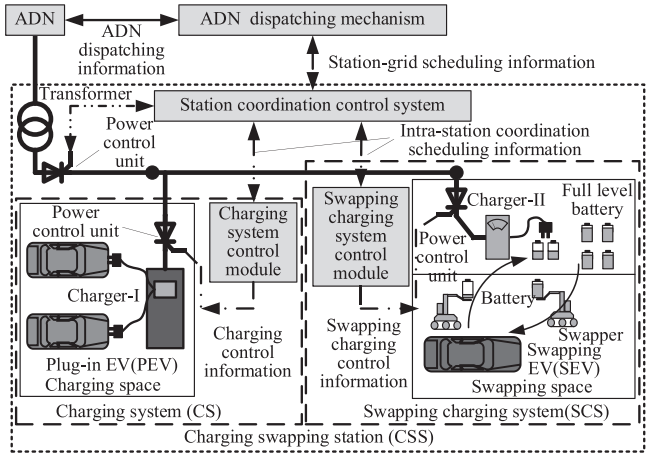

FIGURE 6 The structure of CSS.

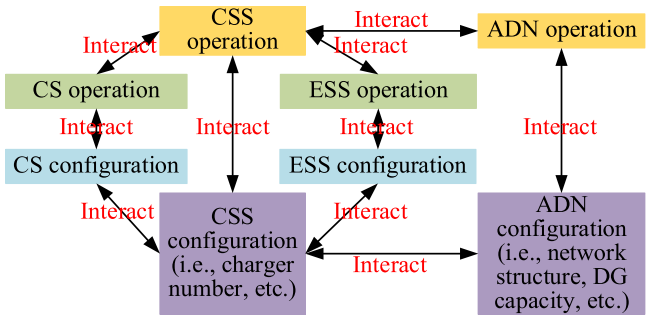

FIGURE 7 The coupling of planning and operation between CSS and ADN.

the EV load number of CSS j at time t; $L^{R}_{j,k}$ is the EV driving distance from road node k to CSS j.

3 | CONFIGURATION MODELS OF CSS AND ADN

3.1 | CSS operation and configuration models

The typical structure of a CSS is shown in Figure 6. The CS is equipped with chargers of specific type (indicated as charger-I) to meet the PEV charging demands and the SCS is equipped by the swappers, the swapping batteries ES and chargers of specific type II, indicated as charger-II.

As the redundancy and margin of the system need to be considered in the planning process, the presence of energy storage in CSS is evaluated so to meet the needs of EV load demands in normal times. The internal energy storage of CSS can also be used to help the ADN in case of congestions or after faults, serving as an emergency power source.

The centralized communication and control of EV charging in CSFs by the grid is of low cost and low complexity with respect to the implementation of the aggregators, demand response schemes, and local markets for the dispatch of dispersed EV charging. Therefore, here, the CSS operation is considered to be scheduled by the utility.

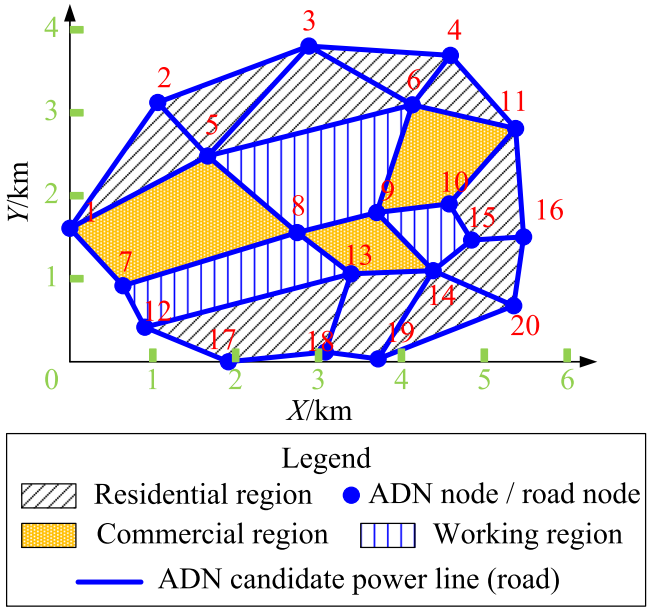

FIGURE 8 Planning area.

TABLE 1 The basic load of ADN nodes.

Node	Power (MW)	Node	Power (MW)	Node	Power (MW)
1	0.5	8	1	15	0.8
2	1	9	0.8	16	0.5
3	0.4	10	0.4	17	0.5
4	0.6	11	0.5	18	0.4
5	0.5	12	1	19	0.6
6	0.5	13	0.5	20	0.4
7	0.4	14	0.6		

3.1.1 | Operation model of CSS

The operation model of CSS is built based on the CS and SCS models. Thus, the CSS i power $P^{\mathrm{CSS}}_{i,t}$ at time t is equal to the sum of CS and SCS:

$$P^{\mathrm{CSS}}_{i,t} = P^{\mathrm{CS}}_{i,t} + P^{\mathrm{SCS}}_{i,t} \tag{18}$$

where $P^{\mathrm{CS}}_{i,t}$ and $P^{\mathrm{SCS}}_{i,t}$ are the power of CS and SCS, respectively.

1. CS operation

The CS operation model is given by (19)–(22):

(19) is the relationship between the CS power $P^{\mathrm{CS}}_{i,t}$ and charger-I's power P^{CI}_{t} in CSS i at time t;

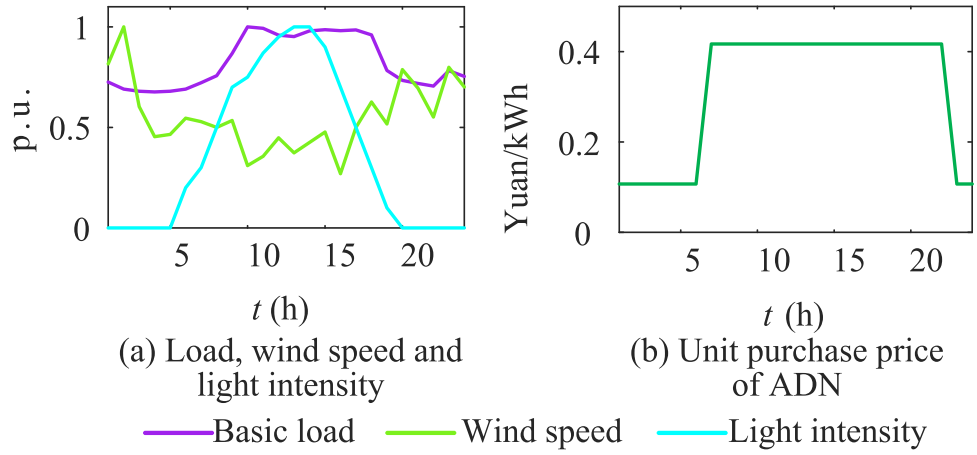

FIGURE 9 Basic parameters.

(20) provides the PEV's maximum charging duration $\Delta t_{\max}^{\mathrm{PEV}}$;
(21) is the relationship between PEV's operating battery level $E_t^{\mathrm{PEV,o}}$ and charging power;
(22) represents the power states of charger-I.

$$P_{i,t}^{\mathrm{CS}} = N_{i,t}^{\mathrm{PEV}} P_t^{\mathrm{CI}}, 0 \le P_t^{\mathrm{CI}} \le P_{\max}^{\mathrm{CI}} \tag{19}$$

$$\frac{E_{\max}^{\mathrm{PEV,o}} - E_{\min}^{\mathrm{PEV,o}}}{\Delta T \eta_{\mathrm{ch}}^{\mathrm{CH}}} \le \sum_{t=t_0^{\mathrm{PEV}}}^{t_0^{\mathrm{PEV}}+\Delta t_{\mathrm{PEV}}} P_t^{\mathrm{CI}}, 0 \le \Delta t_{\mathrm{PEV}} \le \Delta t_{\max}^{\mathrm{PEV}} \tag{20}$$

$$E_t^{\mathrm{PEV,o}} = E_{t-1}^{\mathrm{PEV,o}} + \Delta T P_{t-1}^{\mathrm{CI}} \eta_{\mathrm{c}}^{\mathrm{CH}} \tag{21}$$

$$\begin{cases} P_t^{\mathrm{CI}} \ge 0, E_{\min}^{\mathrm{PEV,o}} \le E_t^{\mathrm{PEV,o}} \le E_{\max}^{\mathrm{PEV,o}} \\ P_t^{\mathrm{CI}} = 0, E_t^{\mathrm{PEV,o}} > E_{\max}^{\mathrm{PEV,o}} \end{cases} \tag{22}$$

In (19)–(22) $P_{\max}^{\mathrm{CI}}$ is the charger-I maximum power [43]; $E_{\max}^{\mathrm{PEV,o}}$ and $E_{\min}^{\mathrm{PEV,o}}$ are the upper and lower limits of battery level of PEV [27]; ΔT is the unit duration [33]; $\eta_{\mathrm{c}}^{\mathrm{CH}}$ is the charging efficiency [39, 44, 61]; t_0^{PEV} and Δt_{PEV} are the charging initial time and duration of a PEV, respectively.

1. SCS operation

The SCS operation model is given by (23)–(28):
(23) is the relationship among SCS i power $P_{i,t}^{\mathrm{SCS}}$ and charging power $P_{i,j,t}^{\mathrm{CII,c}}$ and discharging power $P_{i,j,t}^{\mathrm{CII,d}}$ of charger-II j;
(24) and (25) represent the states and upper limit $P_{\max}^{\mathrm{CII}}$ [43] of charger-II's power, respectively;
(26) represents the coupling between battery level and power of battery;
(27) is the relationship among SCS i power, battery level $E_{i,t}^{\mathrm{SCS,o}}$ and EV load at time t;
(28) gives the number of SCS high-level batteries $N_{i,t}^{\mathrm{SCS,h}}$.

$$P_{i,t}^{\mathrm{SCS}} = \sum_{j=1}^{N_i^{\mathrm{CII}}} \left[P_{i,j,t}^{\mathrm{CII,c}} - P_{i,j,t}^{\mathrm{CII,d}} \right], P_{i,j,t}^{\mathrm{CII,c}} P_{i,j,t}^{\mathrm{CII,d}} = 0 \tag{23}$$

$$\begin{cases} P_{i,j,t}^{\mathrm{CII,c}} = 0, E_{i,j,t}^{\mathrm{SCB,o}} \ge E_{\max}^{\mathrm{SCB,o}} \\ P_{i,j,t}^{\mathrm{CII,d}} = 0, E_{i,j,t}^{\mathrm{SCB,o}} \le E_{\min}^{\mathrm{SCB,o}} \end{cases} \tag{24}$$

$$\begin{cases} 0 \le P_{i,j}^{\mathrm{CII,c}}(t) \le P_{\max}^{\mathrm{CII}}, E_{\min}^{\mathrm{SCB,o}} \le E_{i,j,t}^{\mathrm{SCB,o}} \le E_{\max}^{\mathrm{SCB,o}} \\ 0 \le P_{i,j}^{\mathrm{CII,d}}(t) \le P_{\max}^{\mathrm{CII}}, E_{\min}^{\mathrm{SCB,o}} \le E_{i,j,t}^{\mathrm{SCB,o}} \le E_{\max}^{\mathrm{SCB,o}} \end{cases} \tag{25}$$

$$E_{i,j,t}^{\mathrm{SCB,o}} = E_{i,j,t-1}^{\mathrm{SCB,o}} + \Delta T \left(\eta_{\mathrm{c}}^{\mathrm{CH}} P_{i,j,t-1}^{\mathrm{CII,c}} - \frac{P_{i,j,t-1}^{\mathrm{CII,d}}}{\eta_{\mathrm{d}}^{\mathrm{CH}}} \right) \tag{26}$$

$$E_{i,t}^{\mathrm{SCS,o}} = E_{i,t-1}^{\mathrm{SCS,o}} + \sum_{j=1}^{N_i^{\mathrm{CII}}} E_{i,j,t}^{\mathrm{SCB,o}} + \Delta T \sum_{j=1}^{N_i^{\mathrm{CII}}} \left(\eta_{\mathrm{c}}^{\mathrm{CH}} P_{i,j,t-1}^{\mathrm{CII,c}} - \frac{P_{i,j,t-1}^{\mathrm{CII,d}}}{\eta_{\mathrm{d}}^{\mathrm{CH}}} \right) - \left(E_{\max}^{\mathrm{SCB,o}} - E_{\min}^{\mathrm{SCB,o}} \right) N_{i,t-1}^{\mathrm{SEV}} \tag{27}$$

$$\mathrm{ceil}\{(1+\beta_{\mathrm{SEV}}) N_{i,t}^{\mathrm{SEV}}\} \le N_{i,t}^{\mathrm{SCS,h}} \tag{28}$$

In (23)–(28) E_i^{SCS} is the ES capacity of SCS in CSS i; N_i^{CII} is the number of charger-IIs in CSS i; β_{SEV} is the SEV load margin coefficient; $E_{i,j,t}^{\mathrm{SCB,o}}$ is the battery level of battery j in SCS i at time t.

3.1.2 | Configuration model of CSS

The optimal configuration of CSS is obtained from the configuration models of CS and SCS, provided by (29)–(32).

1. CS configuration

TABLE 2 System parameters.

Parameter	Value	Parameter	Value
β_{CO2}(ton/kWh)	1.08×10^{-3}	Z_{CII}	4
e_{PEV}(kWh/km)	0.25	$S^{WT}_{max}/S^{PV}_{max}$(kVA)	2000
e_{SEV}(kWh/km)	0.25	β_S	0.6
E^{PEV}_{max}(kWh)	50	a_{CI}(m^2)	25
Δt^{PEV}_{max}(h)	1	$S_{i,j,max}$(MVA)	8
a_{SCS}(m^2/kWh)	0.2	c_{CO2}(kYuan/ton)	0.13
β_{CI}	0.2	χ_T	0.75
a_{SW}(m^2)	50	a_{CII}(m^2)	10
β_{SEV}	0.5	$S^{WT}_{min}/S^{PV}_{min}$(kVA)	1000
P_{SW}(kW)	15	β_T	0.2
β_{SW}	0.2	$\cos\phi_{DG}$	1

TABLE 3 Average driving speeds of EVs.

Time	Upper limit of EV average speed (km/h)	Lower limit of EV average speed (km/h)
Traffic restriction period (7:00–9:00)	40	16
Non-traffic restriction period (17:00–19:00)	64	32

TABLE 4 Different planning cases.

Case	CSF type (Coordinated planning with ADN)	CSF characteristic
Case1	Two CSSs	EV integrated multi-function CSF
Case2	One charging station, and one swapping station	EV distributed single function CSF

For the CS configuration, the margin of charger-I is considered, and the number of charger-I N_i^{CI} in CSS i satisfies:

$$\text{ceil}\left\{(1+\beta_{CI})N_{i,t}^{PEV}\right\} \le N_i^{CI} \tag{29}$$

where β_{CI} is the margin coefficient of charger-Is; ceil$\{x\}$ means the x is rounded upper by the units of 1.

1. SCS configuration

For SCS configuration, the capacity of SCS meets:

$$E_{SEV}\text{ceil}\left\{N_{i,t}^{SCS,h}\right\} \le E_i^{SCS} \tag{30}$$

considering that the margin of the equipment, the number of charger-II N_i^{CII} and swappers N_i^{SW} of CSS i meet (31) and (32), respectively.

$$\text{ceil}\left\{\frac{E_i^{SCS}}{Z_{CII}E_{SEV}}\right\} \le N_i^{CII} \tag{31}$$

$$\text{ceil}\left\{\left(1+\beta_{SW}\right)N_{i,t}^{SEV}\right\} \le N_i^{SW} \tag{32}$$

In (31) and (32) Z_{CII} is the number of batteries that can be charged by a charger-II simultaneously; Z_{SW} is the number of SEVs that can be swapped by a swapper within ΔT.

3.2 | Configuration model of ADN

The ADN network topology planning is modelled as a programming problem with mixed integer variables. The power line length matrix $\boldsymbol{D}$ satisfies (33). The ADN matrix $\boldsymbol{Z}$ shows the states of the branches. The radial network constraint of ADN is (34).

$$\overbrace{\begin{bmatrix} D_{1,1} & D_{1,2} & \cdots & D_{1,n} \\ D_{2,1} & D_{2,2} & \cdots & D_{2,n} \\ \vdots & \vdots & \ddots & \vdots \\ D_{n,1} & D_{n,2} & \cdots & D_{n,n} \end{bmatrix}}^{D} \overset{\text{Mapping}}{\Leftrightarrow} \overbrace{\begin{bmatrix} Z_{1,1} & Z_{1,2} & \cdots & Z_{1,n} \\ Z_{2,1} & Z_{2,2} & \cdots & Z_{2,n} \\ \vdots & \vdots & \ddots & \vdots \\ Z_{n,1} & Z_{n,2} & \cdots & Z_{n,n} \end{bmatrix}}^{Z} \tag{33}$$

$$\sum Z_{i,j} = N_{ADN} - 1, \forall i, \forall j \tag{34}$$

where $D_{i,j}$ is the candidate power line length between adjacent node i and j (i.e. $D_{i,j} = \infty$ means that the line cannot be built and $D_{i,j} = 0$ means node i and node j are coincident). $Z_{i,j} = 1/0$ means that the power line between node i and j is proposed/not proposed. N_{ADN} is the numbers of ADN nodes.

Based on the power outputs of DGs (e.g. wind turbine (WT) and photovoltaic (PV) units [47]), the capacity of DGs meet the following limits:

$$0 \le P_t^{DG} \le P_t^{DG,c} \le \frac{S_{DG}}{\cos\phi_{DG}},$$
$$S_{min}^{DG} \le S_{DG} \le S_{max}^{DG} \tag{35}$$

where P_t^{DG} and $P_t^{DG,c}$ are the DG actual power output and upper limit [47] at time t respectively; S_{DG}, S_{max}^{DG} and S_{min}^{DG} are the DG capacity, its upper and lower limits, respectively.

4 | COORDINATED PLANNING MODEL OF CSS AND ADN

The coupling of planning and operation between CSS and ADN is shown in Figure 7.

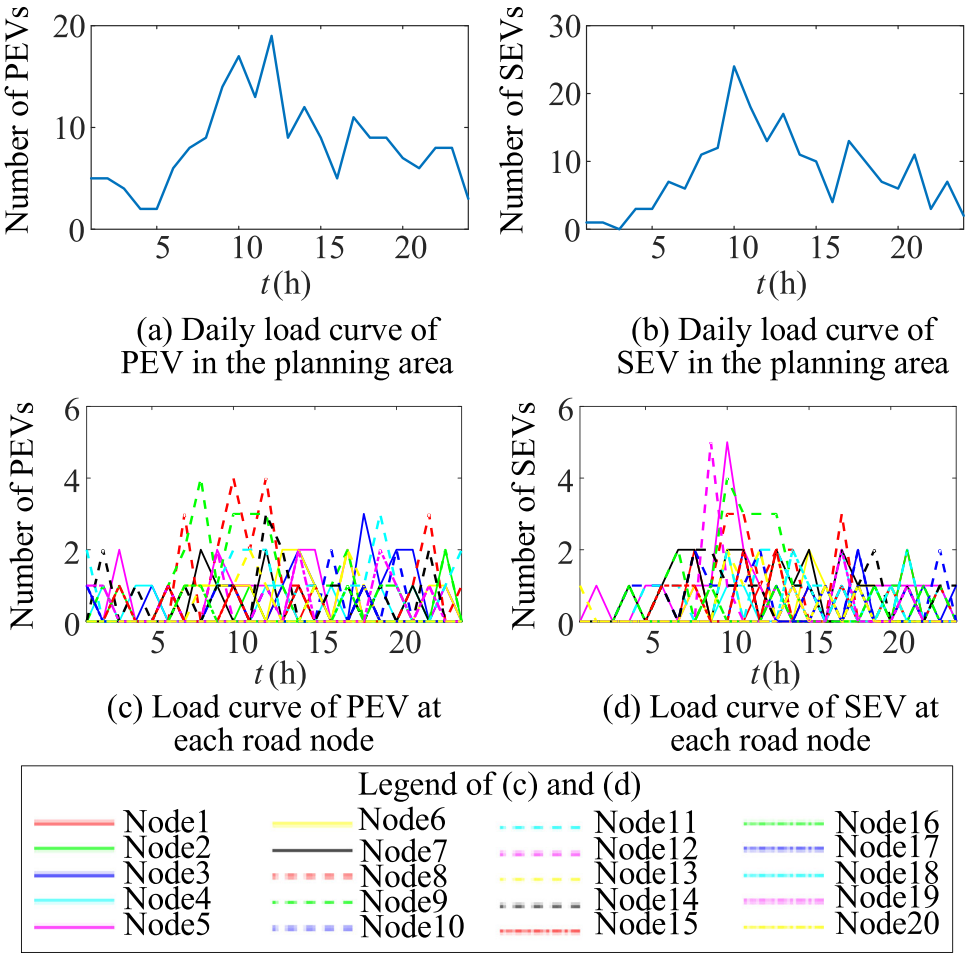

FIGURE 10 The number of EV load forecasting results.

TABLE 5 Comparison alternative schemes.

Cost (k Yuan)	Case1	Case2
Annual comprehensive cost	33781.2218	33541.4203
Construction cost	8360.6060	8282.1708
Energy purchase cost	24158.630	24001.169
Operation-maintenance cost	1253.3071	1246.6071
Carbon trading cost of EV	8.6793	11.4731

4.1 | Objective

Aiming at minimizing the annual comprehensive cost, the objective of the coordinated planning model of CSS and ADN is:

$$\min F = C_{\mathrm{I}} + C_{\mathrm{E}} + C_{\mathrm{O}} + C_{\mathrm{C}} \tag{36}$$

where F includes the infrastructure cost C_{I}, energy purchase cost C_{E}, operation-maintenance (OM) cost C_{O} and EV carbon transaction cost C_{C}.

Considering the optimal configurations of DG, power lines, and CSS, the infrastructure cost is given by:

$$C_{\mathrm{I}} = \sum_{d\in\Phi_{\mathrm{DG}}} \frac{\beta(1+r)^{Y_{\mathrm{DG}}}}{(1+\beta)^{Y_{\mathrm{DG}}}-1} c_d^{\mathrm{DG}} S_d^{\mathrm{DG}} + \sum_{l\in\Phi_{\mathrm{LI}}} \frac{\beta(1+\beta)^{Y_{\mathrm{LI}}}}{(1+\beta)^{Y_{\mathrm{LI}}}-1} c_l^{\mathrm{LI}} D_l^{\mathrm{LI}} + \sum_{s\in\Phi_{\mathrm{SU}}} \frac{\beta(1+\beta)^{Y_{\mathrm{SU}}}}{(1+\beta)^{Y_{\mathrm{SU}}}-1} c_s^{\mathrm{SU}} S_s^{\mathrm{SU}} + \sum_{c\in\Phi_{\mathrm{CSS}}} \sum_{e\in\Phi_{\mathrm{EQ}}} \frac{\beta(1+\beta)^{Y_e^{\mathrm{CSS}}}}{(1+\beta)^{Y_e^{\mathrm{CSS}}}-1} c_{c,e}^{\mathrm{CSS}} S_{c,e}^{\mathrm{CSS}} \tag{37}$$

where β is the discount rate [27]; Y_{DG}, Y_{LI}, Y_{SU}, and Y_e^{CSS} are the service life of DG, power line, substation, and CSS equipment e, respectively [30]; D is the number of days per year [62]; S_d^{DG}, D_l^{LI}, S_s^{SU}, and $S_{c,e}^{\mathrm{CSS}}$ are the capacities/size of DG d, power line l, substation s, and CSS equipment e, respectively; c_d^{DG}, c_l^{LI}, c_s^{SU}, and $c_{c,e}^{\mathrm{CSS}}$ are the unit costs of DG d, power line l, substation s, and CSS equipment e, respectively; Φ_{DG}, Φ_{LI}, Φ_{SU}, Φ_{CSS}, and Φ_{EQ} are the sets of DG, power lines, substations, and CSS equipment, respectively.

The electricity consumption of CSS and basic load, as well as the network losses and DG power outputs, are included in cost C_{E} given by:

$$C_{\mathrm{E}} = D\Delta t \left\{ \sum_{t=1}^{T} c_t^{\mathrm{E}} \left[\sum_{c\in\Phi_{\mathrm{CSS}}} P_{c,t}^{\mathrm{CSS}} + \sum_{k\in\Phi_{\mathrm{LOAD}}} P_{k,t}^{\mathrm{L}} - \sum_{d\in\Phi_{\mathrm{DG}}} P_{d,t}^{\mathrm{DG}} + P_t^{\mathrm{lo}} \right] \right\} \tag{38}$$

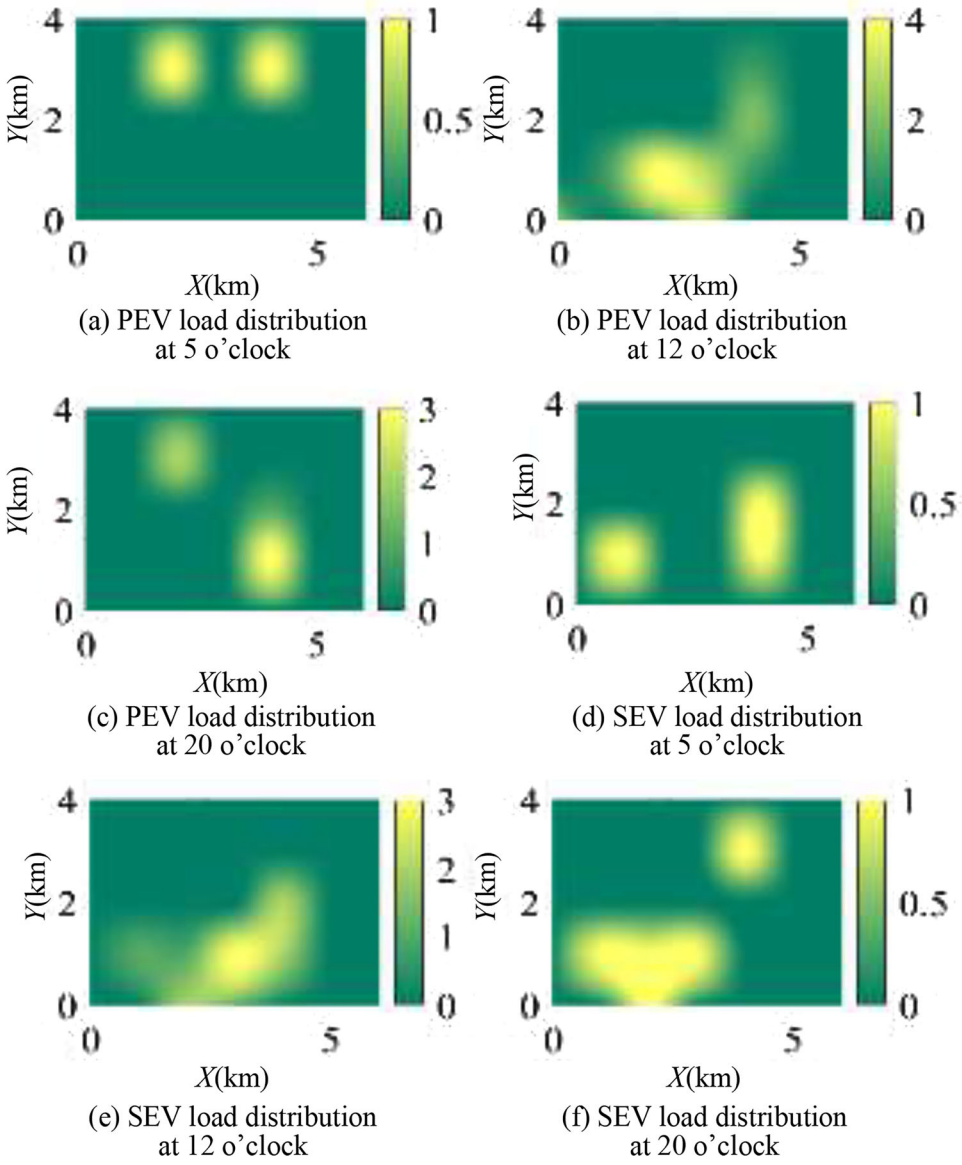

FIGURE 11 The EV spatial-temporal load forecasting results.

where c_t^E is the power purchase price of ADN at time t; $P_{c,t}^{\mathrm{CSS}}$ and $P_{k,t}^{L}$ are the powers of CSS i and basic load k, respectively; $P_{d,t}^{\mathrm{DG}}$ is the power outputs of DG d; P_t^{lo} is the network power loss of the ADN; Φ_{LOAD} is the set of basic loads.

Considering each equipment, the system OM cost is calculated by:

$$C_{\mathrm{O}} = \sum_{d\in\Phi_{\mathrm{DG}}} o_d^{\mathrm{DG}} S_d^{\mathrm{DG}} + \sum_{l\in\Phi_{\mathrm{LI}}} o_l^{\mathrm{LI}} D_l^{\mathrm{LI}} + \sum_{s\in\Phi_{\mathrm{SU}}} o_s^{\mathrm{SU}} S_s^{\mathrm{SU}} + \sum_{c\in\Phi_{\mathrm{CSS}}} \sum_{e\in\Phi_{\mathrm{EQ}}} o_{c,e}^{\mathrm{CSS}} S_{c,e}^{\mathrm{CSS}} \tag{39}$$

where o_d^{DG}, o_l^{LI}, o_s^{SU}, and $o_{c,e}^{\mathrm{CSS}}$ are the annual OM costs of DG d, power line l, substation s, and CSS equipment e, respectively.

The annual EV carbon transaction cost is calculated by:

$$C_{\mathrm{C}} = D c_{\mathrm{CO2}} E_{\mathrm{CO2}} \tag{40}$$

where c_{CO2} is the unit carbon transaction cost.

4.2 | Constraints

4.2.1 | ADN constraints

The ADN operation is represented by the Dist-flow Equation (41). The node voltage constraints meet (42) and the power line capacity limit satisfies (43).

TABLE 6 The configuring results of planning project I.

Case	Case1		Case2	
CSF	Charging station	Swapping station	CSS1	CSS2
Charger-I	23	0	11	12
Charger-II	0	11	8	6
Swapper	0	29	16	14
Energy storage (kWh)	0	2150	1200	1000
Transformer (kVA)	1250	1250	1600	1250
Land area (m^2)	575	1990	1395	1260

TABLE 7 The configuring results of planning project II.

Case	Case1	Case2
WT (kW)	2000	2000
PV (kW)	2000	2000
Substation capacity (MW)	16	16
ADN power line length (km)	17.5071	17.5071
EV annual carbon emissions (Ton)	66.7610	88.2544

$$\begin{cases} \sum\limits_{m\in\Omega(j)} P_{j,m,t} = P_{i,j,t} - R_{i,j}\left|I_{i,j,t}\right|^2 - P_{j,t} \\ \sum\limits_{m\in\Omega(j)} Q_{j,m,t} = Q_{i,j,t} - X_{i,j}\left|I_{i,j,t}\right|^2 - Q_{j,t} \\ P_{j,t} = P_{j,t}^{\mathrm{L}} + \sum\limits_{\forall k} P_{k,j,t}^{\mathrm{CSF}} - \sum\limits_{\forall q} P_{q,j,t}^{\mathrm{DG}} \\ Q_{j,t} = Q_{j,t}^{\mathrm{L}} + \sum\limits_{\forall k} Q_{k,j,t}^{\mathrm{CSF}} - \sum\limits_{\forall q} Q_{q,j,t}^{\mathrm{DG}} \\ \left|V_{j,t}\right|^2 = \left|V_{i,t}\right|^2 - 2(P_{i,j,t}R_{i,j} + Q_{i,j,t}X_{i,j}) + (R_{i,j}^2 + X_{i,j}^2)\left|I_{i,j,t}\right|^2 \\ \left|I_{i,j,t}\right|^2 = \frac{P_{i,j,t}^2 + Q_{i,j,t}^2}{\left|V_{i,t}\right|^2} \end{cases} \tag{41}$$

$$P_{i,j,t}^2 + Q_{i,j,t}^2 \le S_{i,j,\max}^2 \tag{42}$$

$$V_i^{\min} \le V_{i,t} \le V_i^{\max} \tag{43}$$

where $\Omega(j)$ is the set of end nodes of branch that headed of the node j; $P_{i,j,t}$ and $Q_{i,j,t}$ are the active, reactive powers of the beginning of branch i,j at time t, respectively; $I_{i,j,t}$ is the current flowing of branch i,j at time t; $R_{i,j}$ and $X_{i,j}$ are the resistance and reactance of branch i,j, respectively; $P_{k,j,t}^{\mathrm{CSF}}$ and $Q_{k,j,t}^{\mathrm{CSF}}$ are the active and reactive powers of CSF k on ADN node j at time t, respectively; $P_{j,t}^{L}$ and $Q_{j,t}^{L}$ are the active power and reactive power of basic load on the ADN node j at time t, respectively; $P_{q,j,t}^{\mathrm{DG}}$ and $Q_{q,j,t}^{\mathrm{DG}}$ are the active power and reactive powers of DG q on ADN node j at time t, respectively; $V_{i,t}$, V_i^{max} and V_i^{min} are the node i voltage and its upper and lower limits [49], respectively; $S_{i,j,\max}$ is the maximum transmission capacity of the power line i,j.

4.2.2 | Transformer capacity constraints

The capacities constraints of CSS transformer and of the main substation are:

$$\begin{cases} \dfrac{(1+\beta_{\mathrm{T}})\beta_{\mathrm{S}}(P_{\max}^{\mathrm{CI}}N_i^{\mathrm{CI}} + P_{\max}^{\mathrm{CII}}N_i^{\mathrm{CII}} + P_{\mathrm{SW}}N_i^{\mathrm{SW}})}{\chi_{\mathrm{T}}\cos\phi_{\mathrm{T}}} \le T_i^{\mathrm{T}} \\ \dfrac{P_{\mathrm{Sub}}^{\max}}{\chi_{\mathrm{T}}\cos\phi_{\mathrm{T}}} \le S_{\mathrm{Sub}},\ T_i^{\mathrm{T}} \in \mathbf{S}_{\mathrm{T}},\ S_{\mathrm{Sub}} \in \mathbf{S}_{\mathrm{T}} \end{cases} \tag{44}$$

where β_{T} and β_{S} are the coefficients of capacity redundancy and load simultaneous of transformer respectively; P_{SW} is the rated power of a swapper; χ_{T} is the load rate; $\mathbf{S}_{\mathrm{T}}$ is the rated capacities set of the transformer [63]; $P_{\mathrm{Sub}}^{\max}$ is the maximum active load power of substation.

4.2.3 | Construction constraints of CSS

The constraints of CSS area, unit area price cost, and CSS i coordinate $(X_i^{\mathrm{CSS}}, Y_i^{\mathrm{CSS}})$ are:

$$a_{\mathrm{SCS}}E_i^{\mathrm{SCS}} + a_{\mathrm{CI}}N_i^{\mathrm{CI}} + a_{\mathrm{CII}}N_i^{\mathrm{CII}} + a_{\mathrm{SW}}N_i^{\mathrm{SW}} \le A_i^{\mathrm{A}} \le A_i^{\mathrm{S}} \tag{45}$$

$$\begin{aligned} c_i^{\mathrm{A}} &= c_j^{\mathrm{S}},\ (X_i^{\mathrm{CSS}}, Y_i^{\mathrm{CSS}}) \\ &= (X_j^{\mathrm{CSS,S}}, Y_j^{\mathrm{CSS,S}}), (X_i^{\mathrm{CSS}}, Y_i^{\mathrm{CSS}}) \in \mathbf{CSS} \end{aligned} \tag{46}$$

where a_{CI}, a_{CII} and a_{SW} are the areas of a charger-I, charger-II, and swapper, respectively; a_{SCS} is the area of unit capacity ES; A_i^{S} is the planning area upper limit of CSS i; c_j^{S} is the unit area price cost of CSS candidate site j; $(X_j^{\mathrm{CSS,S}}, Y_j^{\mathrm{CSS,S}})$ is the coordinate of CSS candidate site j; ***CSS*** is the CSS candidate coordinates set.

4.3 | Solution approach

The coordinated planning model of CSS and ADN is a large-scale, non-convex, non-linear combinatorial optimization problem, which is difficult to be solved directly. The convex relaxation method is applied to transform the non-convex non-linear energy flow equations (as described in [35, 49] and references therein). Then, the proposed planning is represented by a second-order cone optimization model that can be efficiently solved by the CPLEX solver [49].

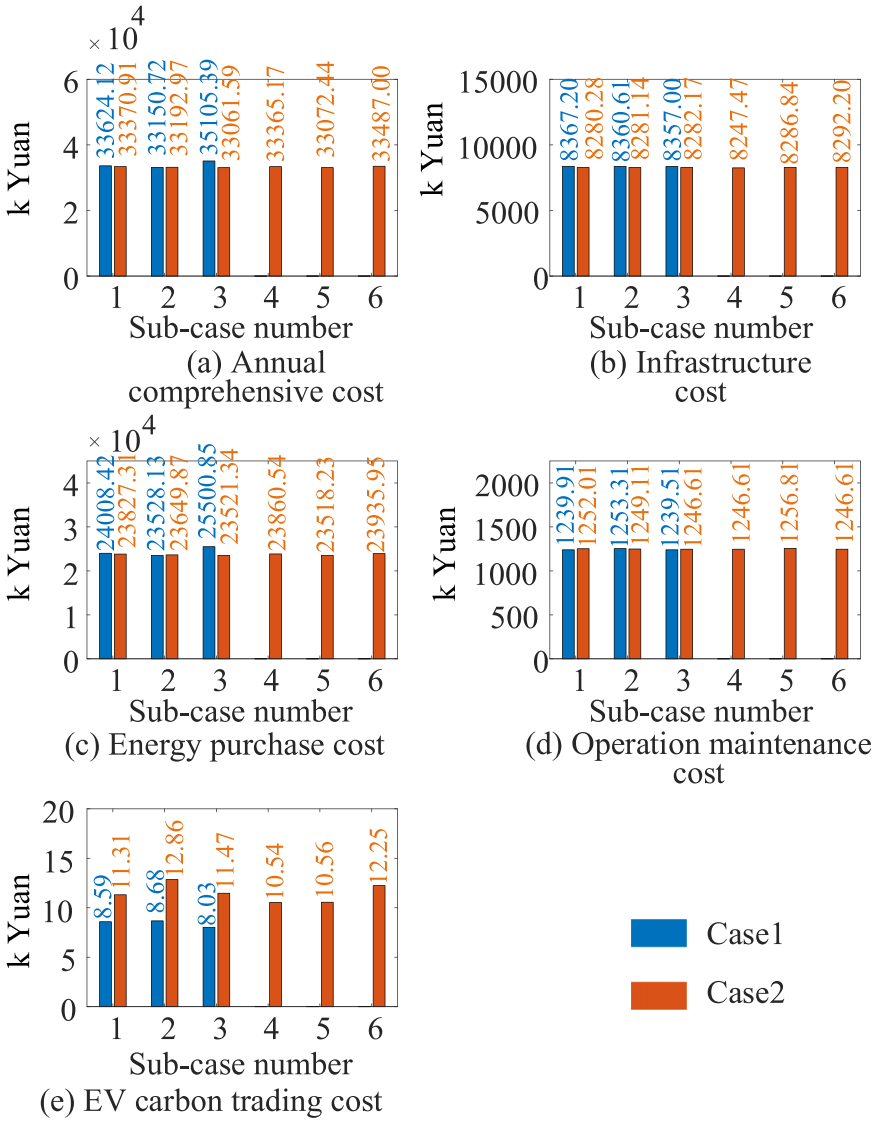

FIGURE 12 The economies of planning project.

5 | CASE STUDY

5.1 | Parameter setting

An actual planning area in eastern China is taken as the case study, which is illustrated in Figure 8. The basic load of ADN nodes is shown in Table 1. The planning profiles and parameters are given in Figure 9 and Table 2. The connection nodes of WT and PV units are node 2 and node 12, respectively. The candidate sites 1 to 3 for CSF installations are located at nodes 5, 8, and 6, respectively. The unit land prices of candidate sites 1 to 3 are 0.22, 0.18, and 0.2 kYuan/m^2, respectively. The substation is located at node 8.

The unit purchase costs for WT unit, PV unit, power line, substation, charger-I, charger-II, swapper, CSF transformer, and swapping energy storage are 3 kYuan/kVA, 5 kYuan/kVA, 500 kYuan/km, 3 kYuan/kVA, 150 kYuan, 100 kYuan, 200 kYuan, 0.25 kYuan/kVA, and 1 kYuan/kWh, respectively. The corresponding unit OM costs are 0.1 kYuan/kVA, 0.2 kYuan/kVA, 1 kYuan/km, 0.03 kYuan/kVA, 0.5 kYuan, 0.2 kYuan, 0.1 kYuan, 0.01 kYuan/kVA, and 0.05 kYuan/kWh, respectively.

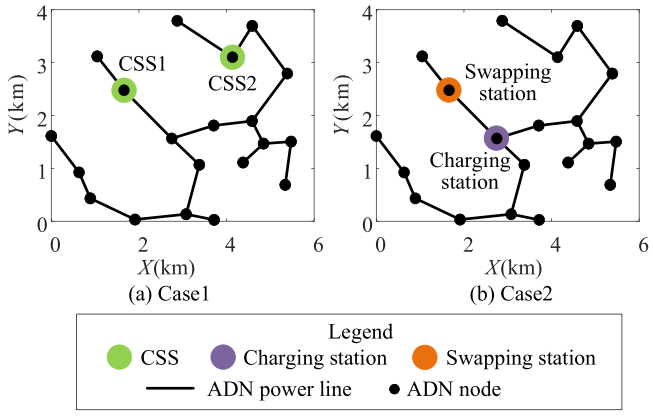

FIGURE 13 The planning results of ADN topology and EV CSFs locations.

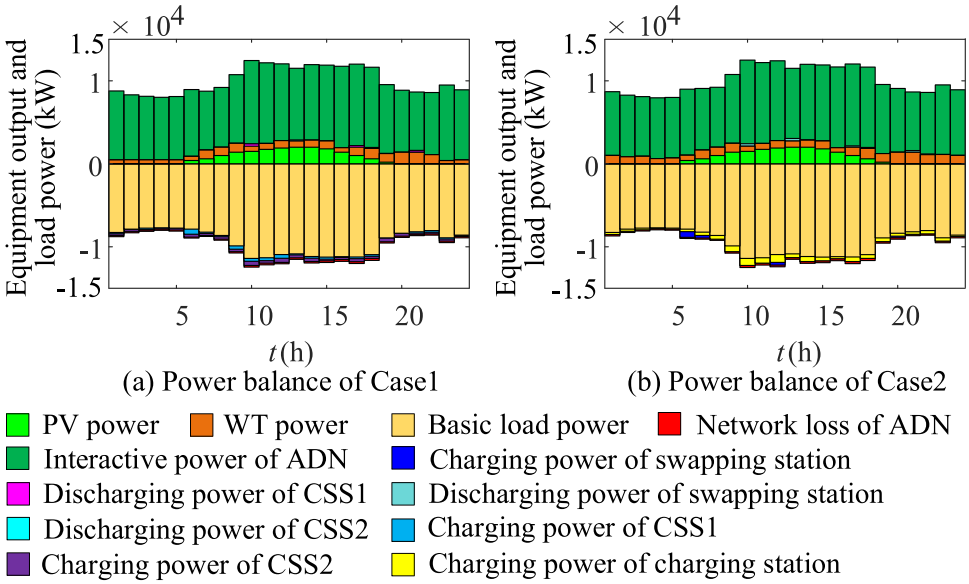

FIGURE 14 The planning results of ADN topology and EV CSFs locations.

The system rated voltage is 10 kV. The per unit length resistance and reactance of a cable are 0.4 and 0.325 Ω/km respectively. Daily total loads numbers of PEVs and SEVs are both 200 in the planning area. The maximum wind speed is 25 m/s. The minimum capacities unit of PV and WT are both 200 kVA. The parameters and data of this test case have been mainly collected from the reports of China State Grid Corporation.

The actual driving speeds of EVs are closely related to the actual traffic conditions. According to the traffic restriction periods and the maximum speed limit of main road equal to 80 km/h in Shanghai, China, the average driving speeds of EVs is shown in Table 3.

To compare and analyze the differences in planning and operation results between EV distributed single function CSFs and EV integrated multi-function CSFs, two planning cases are considered, described in Table 4.

5.2 | Simulation analysis

The EV spatial-temporal load forecasting results are shown in Figures 10 and 11. The spatial-temporal distribution characteristics of EV loads have strong uncertainty and randomness. Since the user habits of PEVs and SEVs are basically identical, the load curves of PEVs and SEVs have a certain similarity. However, since the SEV swapping process is more flexible in temporal than that of the PEV charging process (i.e. the swapping process can occur during both travel and parking periods, but the charging process occurs during parking period), the load forecasting results between PEVs and SEVs show certain differences in time and space.

In Figure 10, the distributions of PEVs and SEVs (i.e., charging and swapping EVs) load demands have strong fluctuations on the timeline. The peak load demands of PEVs and SEVs mainly occur during the daytime. Around 12:00, many EVs depart from RRs to WRs or CRs, resulting in a load superposition and an early peak load occurrence. The largest number of PEVs and SEVs are 19 and 24 respectively. At about 20:00, most PEVs and SEVs return to RRs and cause an evening peak load. By the EV spatial-temporal load forecasting method proposed in this paper, the temporal distribution curve EV load for each road node is obtained, as shown in Figure 10.

Figure 11 (relevant to few typical EV spatial-temporal distributions) illustrates the uncertainty, randomness, imbalance etc., of temporal and spatial distribution characteristics of PEVs and SEVs loads. At 5:00, the PEVs and SEVs loads concentrate in RRs mainly. At about 12:00, the loads concentrate on WRs and CRs mainly. The EV loads are generated to randomly spread all over the planning area (i.e. RRs, WRs, and CRs) at about 20:00. As a result, the EV spatial-temporal load analysis and forecasting method based on the travel chains theory proposed here can reasonably reflect the spatial-temporal dynamic change rule and uncertainty of driving, parking, and other states during EV travel. The results of EV spatial-temporal loads are used as the basis of the CSS planning.

Figure 12 shows the economic aspects of the planning project. It can be seen from Figure 12, for the planning of CSS and ADN (i.e. in Case 1), the annual comprehensive cost (F) of planning Case 1-2 is lower than that of Cases 1-1 and 1-3 respectively. Thus, Case 1-2 is the best among the sub-cases of Case 1. For the planning of charging, swapping stations, and ADN in Case 2, the F of Case 2-3 is lowest. Thus, Case 2-3 is the best scheme in Case 2. Cases 1-2 and 2-3 are considered alternative sub-cases to be compared and analyzed.

Table 5 shows the comparison alternative schemes. Case 1-2 in Case 1 and Case 2-3 in Case 2 are indicated as Case 1 and Case 2 in the following text, respectively, for simplicity. Although

FIGURE 15 The planning results of ADN topology and EV CSFs locations.

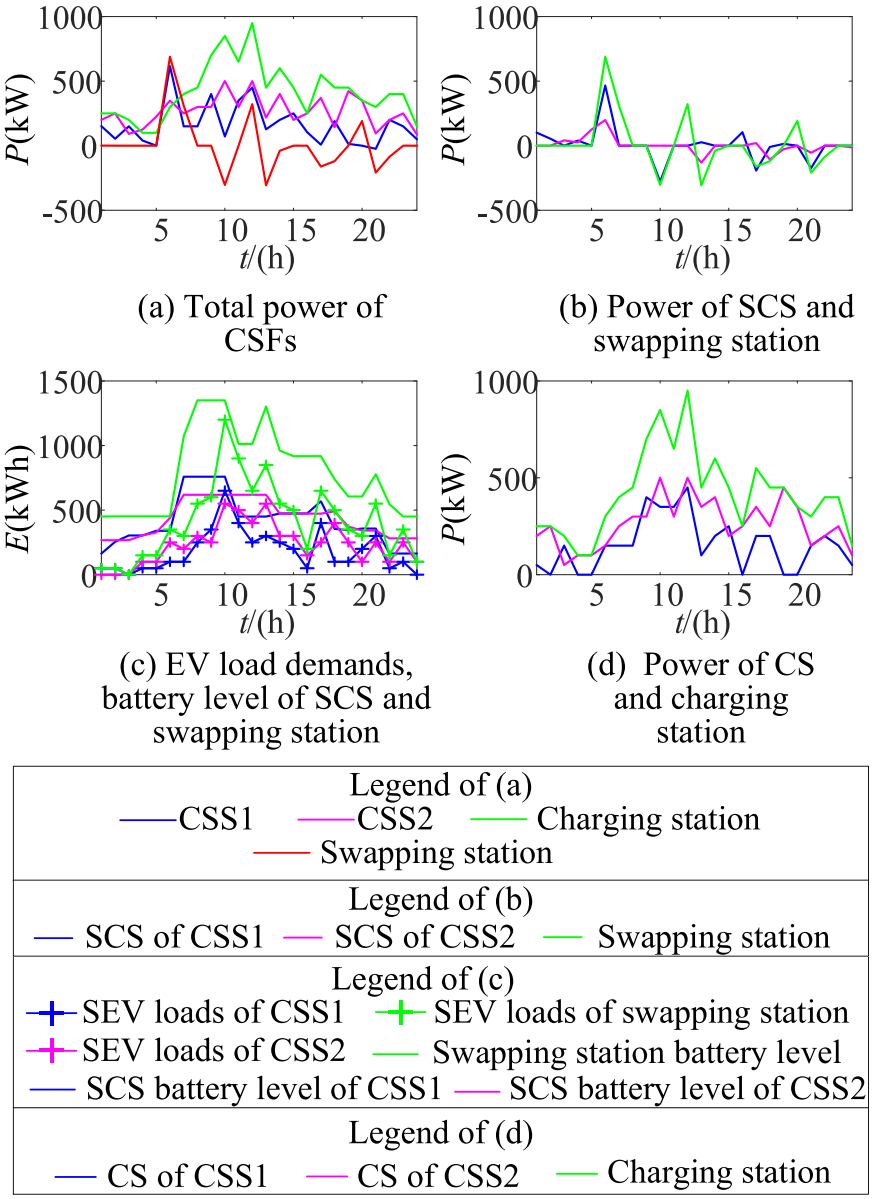

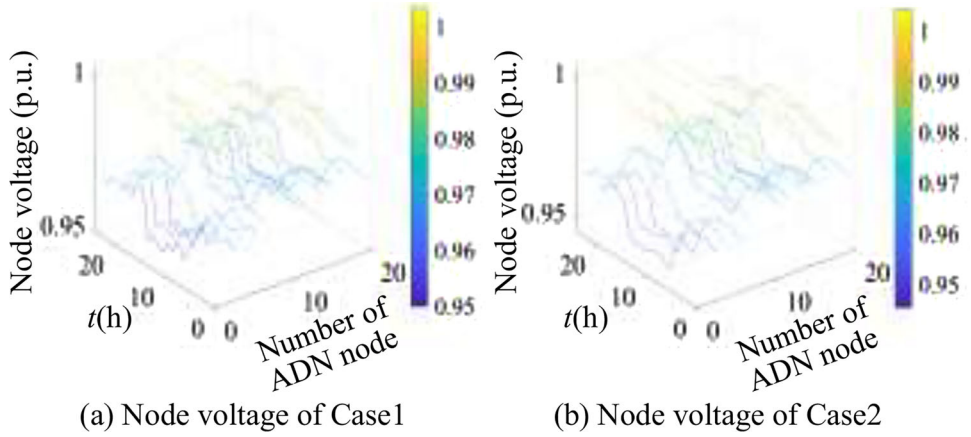

FIGURE 16 The voltages of ADN nodes.

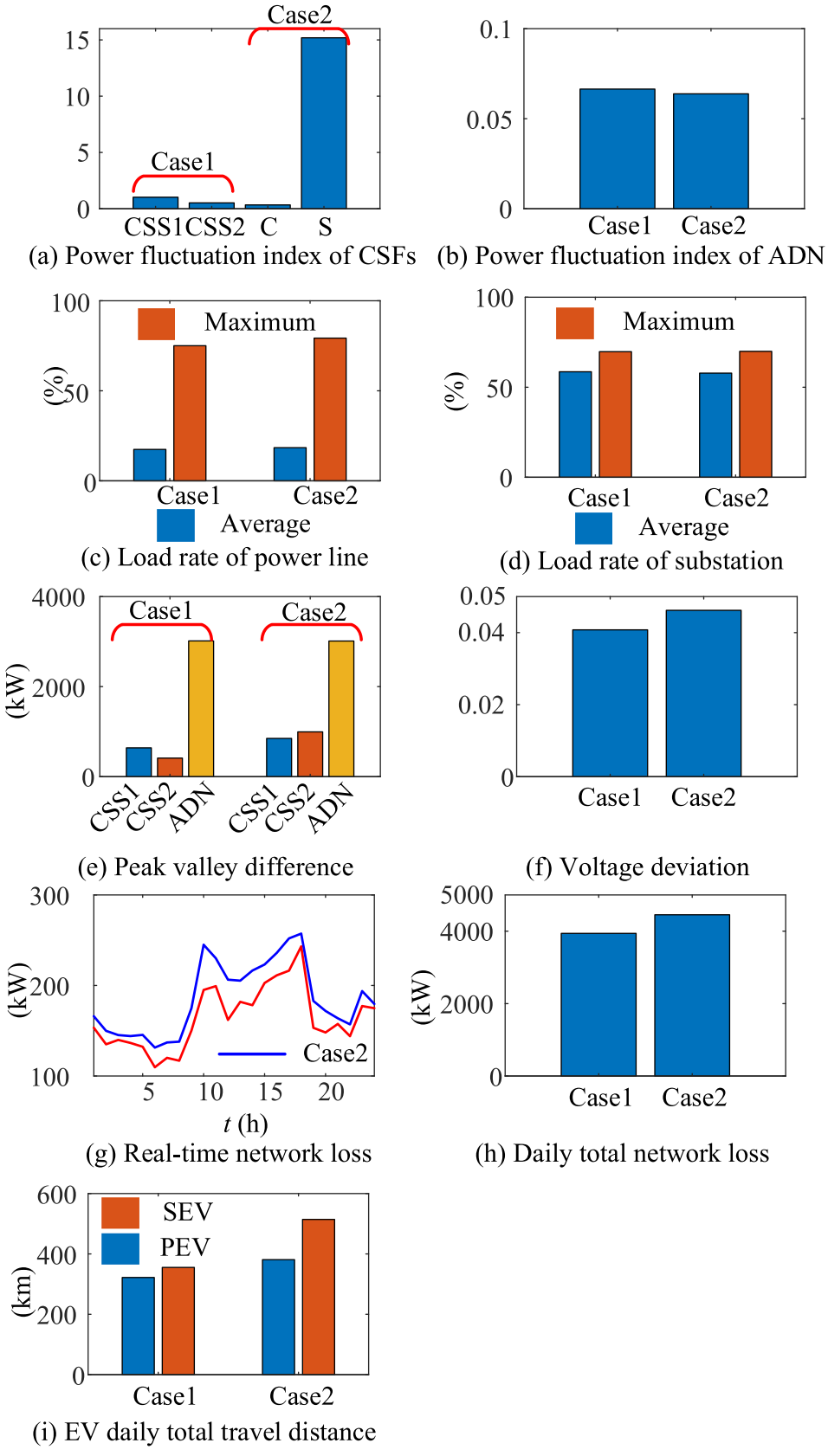

FIGURE 17 The various indexes of planning project.

the types and functions of the selected CSFs have significant differences (i.e. distributed single function units vs centralized multi-function unit), the sizes in the two sub-cases are almost the same. The infrastructure cost of Case 1 is higher than that of Case 2. It has less difference in energy purchase costs between the 2 sub-cases, which is caused by the close EV load levels in the two sub-cases. The OM cost of Case1 is higher than that of Case 2, which is caused by the close overall system planning scales in the two sub-cases. The daily driving distances of EVs for energy supply of Case 1 are shorter, resulting the EV carbon transaction cost of Case 1 lower than in Case 2. Therefore, the planning scale and economy of Case 1 are basically the same as those of Case 2, but the CSSs in Case 1 can reduce the carbon emissions of EVs driving.

Tables 6 and 7 show that the total number of charger-I in CSFs of the two cases are the same. The planning results of ADN topology and EV CSFs locations are shown in Figure 13. The number of charger-II, swapper, SCS ES capacity, transformer capacity, and area of Case1 are 3, 1, 50 kWh, 350 kVA, 90 m^2 larger than those of Case 2, respectively. The corresponding average annual investments of Case 1 are 26.1554, 17.4369, 11.8698, 7.6286, 15.3445 kYuan higher than those of Case 2, respectively. The OM costs of charger-II, swapper, SCS ES, and transformer of Case1 are 0.6000, 0.1000, 2.5000, 3.5000 kYuan higher than those of Case 2, respectively. Therefore, the EV CSFs total planning scales between the two cases have less difference.

With the same construction scales of ADNs in the two cases—that is, the PV capacity of 2000 kVA, WT capacity of 2000 kVA, power line length of 17.5071 km, and substation expansion capacity of 16,000 kVA—the investments of ADNs in the two cases are the same.

The planning scales of CSFs and ADN between Case1 and Case 2 are basically same. ADN optimal topologies in the two cases are the same. The proposed planning method can meet the power supply at all nodes. The annual carbon emission of EV in Case 1 is 21.4934 tonnes less than that of Case 2, which indicates that compared with the charging, and swapping stations, the CSS can further improve the environmental protection.

Figure 14 shows the ADN power balance optimization results. The operation state optimization results of CSFs are shown in Figure 15. Figure 14 shows that the overall ADN power balances of the two cases are basically similar. All kinds of loads, DGs power outputs, and ADN interactive power meet the power balance demands. Figure 15 shows that charging, swapping stations in Case 2 have higher powers compared to the CSSs in Case 1. CSSs can cut down the peak load power of the local grid. The ADN has a larger operation margin. The CSSs and swapping stations reduce the peak power demands as much as possible during the period of high energy purchase price. Figure 15c shows that the operation battery levels of SCSs (CSSs, Case 1) and swapping station (Case 2) are not less than the energy demands of SEV loads in each period.

Figure 16 shows the bus voltages. Various indexes of the planning project are illustrated in Figure 17. Figures 16 and 17 show that although the EV CSFs types of the two cases are different, the node voltages in the two cases both meet the constraints. The minimum node voltages of Case 1 and Case 2 are 0.9498 and 0.9452 p.u., respectively. The maximum node voltages are 1.0035 and 1.0044 p.u., respectively. The voltage deviations, as defined in [64], of Case 1 is 0.0054 lower than that of Case 2. This is because CSS can achieve the complementary operation of the subsystem in the station, improving the power flow distribution and the system voltage profile.

Figure 17 shows that the power fluctuation index of Case 2 charging, and swapping stations are −0.6826 and 14.1692 higher than those of the maximum between CSS1 and CSS2 in Case1, respectively. The power fluctuation index of Case1 is 0.0026 higher than that of Case2, which is a small difference. The CSSs have better EV load fluctuation stabilization capabilities. In terms of average and maximum power line load rate, for Case 2 they are 0.97% and 4.21% higher than those of Case1, respectively. The average and maximum substation load rates of Case 1 are 0.74% and 0.17% lower than those of Case 2, respectively. The peak valley differences of charging, and swapping stations are 210.2 and 355.1 kW higher than those of the maximum between CSS1 and CSS2, respectively. The peak valley differences of Case 2 are 2.8 kW smaller than that of Case 1. The real-time network loss of Case 1 is lower, and the daily total value is 513.6 kW lower than that of Case 2. The total daily driving distance of PEVs and SEVs in Case 2 is 59.11 and 158.98 km higher than that of Case 1 respectively.

6 | CONCLUSION

This paper proposes a coordinated planning method of CSS and ADN considering EV spatial-temporal load forecasting. At first, based on the travel chains analysis of EVs, the EV forecasting model is developed. Then, the configuration model of CSS is built, based on the modelling of CS and SCS. According to the model of ADN network and DG capacities, a coordinated planning model of CSS and ADN is finally developed. The results obtained for realistic test cases support the following conclusions.

1. The adopted EV spatial-temporal load forecasting method can reflect the spatial-temporal dynamic change rule and uncertainty of driving, parking, and other states during EV travels. It describes the charging characteristics and the spatial aggregation and dispersion degree in the planning area at different times.
2. The planning method of CSS and ADN proposed in this paper achieves the sizing and locating planning of CSSs, and the planning results satisfy the PEVs and SEVs load demands in the planning area. The plans the ADN network topology and the capacities of DGs and substations are obtained. The ADN satisfies the load demands of CSSs and basic load nodes, meeting DGs power outputs and grid radial structure constraint.
3. The CSS use can improve the ADN operation. Compared to the single function charging stations and swapping stations, the CSSs have the advantages of multi-function, integration, and subsystem energy complementary operation. As a

result, in the CSSs and ADN coordinated planning, the peak valley differences, ADN network loss, power fluctuation index, power line load rate, EVs driving carbon emissions, and power demands are reduced. The EV use convenience, the ADN transmission margins, and the voltage quality are increased, which improves the safety, reliability, environmental protection and comprehensive economy of the planning.

NOMENCLATURE

Functions

$\mho_i$	Set of road nodes that belong to region i
$\mathbf{CO}_{t,i}^{\mathrm{EV}}(j) = (X_{t,i}^{\mathrm{EV}}(j), Y_{t,i}^{\mathrm{EV}}(j))$	EV j load coordinates
$\mathbf{N}_t^{\mathrm{r,C}}$	EV load mapping matrix between road nodes, CSSs
$\mathbf{N}_t^{C}$	All CSSs EV load numbers set
$\mathbf{N}_t^{r}$	EV load numbers set
$\mathbf{P}_t^{a}$, $\mathbf{P}_t^{r}$	Regions, road nodes EV load demand probabilities matrixes
$\mathbf{S}_{\mathrm{T}}$	Transformer rated capacities set
$\mathbf{SW}_{\mathrm{To}}^{\mathrm{EV}}$, $\mathbf{SW}_{\mathrm{Ty}}^{\mathrm{EV}}$	EV load distribution total, typical scenarios
$\mathbf{SW}_{R}^{\mathrm{EV}}$	Mapping matrix between EV load coordinates with road nodes
$\mathbf{W}_{j,t}^{\mathrm{EV,R}}$	Road node j EV load coordinates
$\mathbf{W}_{t,i}^{\mathrm{EV}}$	EV spatial-temporal load scenario i
$\mathbf{\Phi}_{\mathrm{DG}}$, $\mathbf{\Phi}_{\mathrm{LI}}$, $\mathbf{\Phi}_{\mathrm{SU}}$, $\mathbf{\Phi}_{\mathrm{CSS}}$, $\mathbf{\Phi}_{\mathrm{EQ}}$, $\mathbf{\Phi}_{\mathrm{LOAD}}$	DG, power line, substation, and CSS equipment, basic loads set
CSS	CSS candidate coordinates set
D	Power line length matrix

Indices and Sets

Z	ADN branch states matrix
ceil{*x*}	x is rounded upper by the units of 1
t, T, Δt	Index, hour numbers per day, unit time slot
$\mathbf{CO}_{t,i,j}^{\mathrm{EV}}$	Road node j EV load coordinate i
$\mathbf{\Omega}$(j)	End nodes set of branches headed of node j

Parameters

c_{CO2}	Unit carbon transaction cost
$(X_j^{\mathrm{CSS,S}}, Y_j^{\mathrm{CSS,S}})$	CSS candidate site j coordinate
$\mathcal{A}_i^{\mathrm{S}}$	CSS i planning area upper limit
$D_{i,j}$	Candidate power line length between adjacent node i and j
$E_{\max}^{\mathrm{PEV,o}}$, $E_{\min}^{\mathrm{PEV,o}}$	Upper, lower limits of PEV battery level
$E_{\max}^{\mathrm{PEV}}$, $E_{\max}^{\mathrm{SEV}}$	PEV, SEV ES capacity
N_{a}, N_{r}	Numbers of regions, road nodes
N_{ADN}	Numbers of ADN nodes
N_{CSS}	Number of CSSs
N_{SC}	Numbers of scenario simulated at the same time slot
$P_{\max}^{\mathrm{CI}}$, $P_{\max}^{\mathrm{CII}}$	Charger-I, Charger-II maximum power
$P_{\mathrm{Sub}}^{\max}$	Substation maximum active load power
P_{SW}	Swapper rated power
$P_{i,t}^{a}$, $P_{i,j,t}^{r}$	Region i, road node j EV load demand probabilities
$P_{j,t}^{L}$, $Q_{j,t}^{L}$	ADN node j basic load active, reactive powers
$P_{k,t}^{L}$	Basic load k power
$P_t^{\mathrm{DG,c}}$	DG power output upper limit
$R_{i,j}$, $X_{i,j}$	Branch i,j active, reactive powers
$S_{\max}^{\mathrm{DG}}$, $S_{\min}^{\mathrm{DG}}$	DG capacity upper, lower limits
$S_{i,j,\max}$	Power line i,j maximum transmission capacity
V_i^{max}, V_i^{min}	Node i voltage upper and lower limits
Y_{DG}, Y_{LI}, Y_{SU}, Y_e^{CSS}	DG, power line, substation, CSS equipment e service life
Z_{CII}	Number of batteries that can be charged by a charger-II simultaneously
Z_{SW}	Number of SEVs that can be swapped by a swapper within ΔT
a_{CI}, a_{CII}, a_{SW}, a_{SCS}	Charger-I, charger-II, swapper, unit capacity ES areas
c_d^{DG}, c_l^{LI}, c_s^{SU}, $c_{c,e}^{\mathrm{CSS}}$	DG d, power line l, substation s, CSS equipment e unit cost
c_j^{S}	CSS candidate site j unit area price cost
c_t^{E}	ADN power purchase price
e_{PEV}, e_{SEV}	PEV, SEV energy consumption per unit driving distance
o_d^{DG}, o_l^{LI}, o_s^{SU}, $o_{c,e}^{\mathrm{CSS}}$	DG d, power line l, substation s, CSS equipment e annual OM cost
β_{CI}, β_{SEV}	Margin coefficient of charger-Is, SEV load
β_{CO2}	Carbon emissions per unit of electric energy of traditional generating units
β_{T}, β_{S}	Transformer capacity redundancy, load simultaneous coefficients
$\eta_{\mathrm{c}}^{\mathrm{CH}}$	Charging efficiency
χ_{T}	Load rate
μ, σ	EV driving duration probability parameters
D	Number of days per year
β	Discount rate

Variables

Δt_{D}	EV driving duration between 2 regions
$\Delta t_{\max}^{\mathrm{PEV}}$	PEV's maximum charging duration

A_i^{A}, T_i^T	CSS i area, transformer capacity
$D_{i,j,t}^{\mathrm{PEV,min}}$, $D_{i,k,t}^{\mathrm{SEV,min}}$	PEV j, SEV k drives to CSS i minimum distance
E_{CO2}	The EVs' daily total carbon emission
$E_{i,j,t}^{\mathrm{SCB,o}}$	SCS i battery j battery level
$E_{i,t}^{\mathrm{SCS,o}}$	SCS i battery level
$E_i^{\mathrm{EV,S}}$	EV battery level that accomplishes the driving process I
E_i^{SCS}	CSS i SCS ES capacity
$E_t^{\mathrm{PEV,o}}$	PEV's operating battery level
$I_{i,j,t}$	Branch i,j current flowing
$L_{j,k}^R$	EV driving distance from road node k to CSS j
$N_{R,k,t}^{\mathrm{EV}}$	Number of EVs load at road node k
$N_{i,t}^{\mathrm{PEV}}$, $N_{i,t}^{\mathrm{SEV}}$	Load numbers of PEVs, SEVs of CSS i
$N_{i,t}^{\mathrm{SCS,h}}$	Number of SCS high-level batteries
N_i^{CI}	Number of charger-I
N_i^{CII}	Number of charger-IIs in CSS i
N_i^{CII}, N_i^{SW}	Numbers of charger-IIs, swappers
$N_{j,k,t}^{\mathrm{EV}}$	Number of EV loads mapping between road node k and CSS j
$N_{j,t}^{\mathrm{EV}}$	Number of EV load of CSS j
$N_{t,j}^{\mathrm{EV,R}}$	Number of EV load coordinates that belong to road node j
$P_{i,j,t}$, $Q_{i,j,t}$	Branch i,j active, reactive powers
$P_{i,t}^{\mathrm{CS}}$, P_t^{CI}, $P_{c,t}^{\mathrm{CSS}}$	CS i, charger-I, CSS c powers
$P_{i,t}^{\mathrm{CSS}}$, $P_{w,t}^{\mathrm{WT}}$, $P_{p,t}^{\mathrm{PV}}$	CSS i, WT w and PV p powers
$P_{i,t}^{\mathrm{SCS}}$, $P_{i,j,t}^{\mathrm{CII,c}}$, $P_{i,j,t}^{\mathrm{CII,d}}$	SCS i charger-II j power, charging power, discharging power
$P_{k,j,t}^{\mathrm{CSF}}$, $Q_{k,j,t}^{\mathrm{CSF}}$	ADN node j CSF k active, reactive powers
$P_{q,j,t}^{\mathrm{DG}}$, $Q_{q,j,t}^{\mathrm{DG}}$	ADN node j DG q active, reactive powers
P_t^{DG}, S_{DG}	DG power output, capacity
P_t^{lo}	ADN network power loss
S_d^{DG}, D_l^{LI}, S_s^{SU}, $S_{c,e}^{\mathrm{CSS}}$	DG d, power line l, substation s, and CSS equipment e capacities/amount
$V_{i,t}$	Node i voltage
$V_i^{\mathrm{EV,D}}$	EV driving process i average driving speed
$Z_{i,j}$	Power line building variable between node *i* and *j*
t_0^{PEV}, Δt_{PEV}	PEV charging initial time, duration
$t_{\mathrm{C}}^{\mathrm{PEV}}$, $t_{\mathrm{S}}^{\mathrm{SEV}}$	PEV initial charging, SEV swapping time
t_{L}, Δt_{P}	EV initial departure time, parking duration
t_{P}	Initial parking time that EV just arrived at a region
$t_{\mathrm{S,a}}^{\mathrm{SEV}}$, $t_{\mathrm{S,b}}^{\mathrm{SEV}}$	SEV possible swapping time a and b
z	EV driving process duration intermediate variable
Δt_i^P, Δt_i^D	EV parking duration *i*, driving duration *i*
F, C_{I}, C_{E}, C_{O}, C_{C}	Costs of annual comprehensive, infrastructure, energy purchase, operation-maintenance, EV carbon transaction

AUTHOR CONTRIBUTIONS

Chenke He: Conceptualization, Data curation, Formal analysis, Investigation, Methodology, Software, Validation, Visualization, Writing—original draft. Jizhong Zhu: Funding acquisition, Resources. Alberto Borghetti: Supervision, Writing—review and editing. Yun Liu: Funding acquisition. Shenglin Li: Project administration

ACKNOWLEDGEMENTS

This work was supported by the National Natural Science Foundation of China (52177087), and High-end Foreign Experts Project (G2022163018L), and Science and Technology Projects in Guangzhou under Grant (202201010354).

CONFLICT OF INTEREST STATEMENT

The authors declare no conflicts of interest.

DATA AVAILABILITY STATEMENT

The data that support the findings of this study are available from the corresponding author upon reasonable request.

ORCID

Jizhong Zhu https://orcid.org/0000-0001-5681-1361
Alberto Borghetti https://orcid.org/0000-0002-5011-3324

REFERENCES

1. Zheng, Y., et al.: A systematic methodology for mid-and-long term electric vehicle charging load forecasting: The case study of Shenzhen, China. Sustainable Cities Soc. 56, 102084 (2020)
2. Nogueira, T., Sousa, E., Alves, G.R.: Electric vehicles growth until 2030: Impact on the distribution network power. Energy Rep. 8, 145–152 (2022)
3. Liu, Z., Liu, Z.: Load characteristics forecasting of Hubei power grid up to year 2030 with the development of electric vehicles. Energy Rep. 8, 259–268 (2022)
4. Bao, H., et al.: Relevance vector machine with optimal hybrid kernel function for electric vehicles ownership forecasting: The case of China. Energy Rep. 8, 988–997 (2022)
5. Feng, J., et al.: Load forecasting of electric vehicle charging station based on grey theory and neural network. Energy Rep. 7, 487–492 (2021)
6. Arias, M.B., Bae, S.: Electric vehicle charging demand forecasting model based on big data technologies. Appl. Energy 183, 327–339 (2016)
7. Buzna, L., et al.: An ensemble methodology for hierarchical probabilistic electric vehicle load forecasting at regular charging stations. Appl. Energy 283, 116337 (2021)
8. Tan, B., Chen, H.: Multi-objective energy management of multiple microgrids under random electric vehicle charging. Energy 208, 118360 (2020)
9. Amini, M.H., Kargarian, A., Karabasoglu, O.: ARIMA-based decoupled time series forecasting of electric vehicle charging demand for stochastic power system operation. Electr. Power Syst. Res. 140, 378–390 (2016)
10. Liu, Y., et al.: Prediction of vehicle driving conditions with incorporation of stochastic forecasting and machine learning and a case study in energy

management of plug-in hybrid electric vehicles. Mech. Syst. Sig. Process. 158, 107765 (2021)
11. Jahangir, H., et al.: Charging demand of plug-in electric vehicles: Forecasting travel behavior based on a novel Rough Artificial Neural Network approach. J. Cleaner Prod. 229, 1029–1044 (2019)
12. Wang, N., et al.: A service demand forecasting model for one-way electric car-sharing systems combining long short-term memory networks with Granger causality test. J. Cleaner Prod. 244, 118812 (2020)
13. Gruosso, G., Mion, A., Storti Gajani, G.: Forecasting of electrical vehicle impact on infrastructure: Markov chains model of charging stations occupation. eTransportation 6, 100083 (2020)
14. Dong, X., et al.: A load forecast method for fast charging stations of electric vehicles on the freeway considering the information interaction. Energy Procedia 142, 2171–2176 (2017)
15. Liu, Y., et al.: Fast charging demand forecasting based on the intelligent sensing system of dynamic vehicle under EVs-traffic-distribution coupling. Energy Rep. 8, 1218–1226 (2022)
16. He, L., et al.: A bi-layer optimization based temporal and spatial scheduling for large-scale electric vehicles. Appl. Energy 168, 179–192 (2016)
17. Afshar, M., Mohammadi, M.R., Abedini, M.: A novel spatial–temporal model for charging plug hybrid electrical vehicles based on traffic-flow analysis and Monte Carlo method. ISA Trans. 114, 263–276 (2021)
18. Li, B., et al.: Coordinated scheduling of a gas/electricity/heat supply network considering temporal-spatial electric vehicle demands. Electr. Power Syst. Res. 163, 382–395 (2018)
19. Xiang, Y., et al.: Electric vehicle charging in smart grid: A spatial-temporal simulation method. Energy 189, 116221 (2019)
20. Anand, M.P., Bagen, B., Rajapakse, A.: Probabilistic reliability evaluation of distribution systems considering the spatial and temporal distribution of electric vehicles. Int. J. Electr. Power Energy Syst. 117, 105609 (2020)
21. Yi, T., et al.: Research on the spatial-temporal distribution of electric vehicle charging load demand: A case study in China. J. Cleaner Prod. 242, 118457 (2020)
22. Ge, X., et al.: Data-driven spatial-temporal prediction of electric vehicle load profile considering charging behavior. Electr. Power Syst. Res. 187, 106469 (2020)
23. Ban, M., et al.: Optimal scheduling for electric vehicle battery swapping-charging system based on nanogrids. Int. J. Electr. Power Energy Syst. 130, 106967 (2021)
24. Yang, X., et al.: Deploying battery swap stations for shared electric vehicles using trajectory data. Transp. Res. Part D: Transp. Environ. 97, 102943 (2021)
25. Li, C., et al.: A battery centralized scheduling strategy for battery swapping of electric vehicles. J. Energy Storage 51, 104327 (2022)
26. Wang, H., et al.: Optimal scheduling of electric vehicles charging in battery swapping station considering wind- photovoltaic accommodation. Electr. Power Syst. Res. 199, 107451 (2021)
27. Zeng, B., Luo, Y., Liu, Y.: Quantifying the contribution of EV battery swapping stations to the economic and reliability performance of future distribution system. Int. J. Electr. Power Energy Syst. 136, 107675 (2022)
28. Li, Y., et al.: Optimal scheduling of isolated microgrid with an electric vehicle battery swapping station in multi-stakeholder scenarios: A bi-level programming approach via real-time pricing. Appl. Energy 232, 54–68 (2018)
29. Xu, X., et al.: Robust energy management for an on-grid hybrid hydrogen refueling and battery swapping station based on renewable energy. J. Cleaner Prod. 331, 129954 (2022)
30. Domínguez-Navarro, J.A., et al.: Design of an electric vehicle fast-charging station with integration of renewable energy and storage systems. Int. J. Electr. Power Energy Syst. 105, 46–58 (2019)
31. Dong, H., et al.: Capacity planning and pricing design of charging station considering the uncertainty of user behavior. Int. J. Electr. Power Energy Syst. 125, 106521 (2021)
32. Liu, J., et al.: A planning strategy considering multiple factors for electric vehicle charging stations along German motorways. Int. J. Electr. Power Energy Syst. 124, 106379 (2021)
33. Rezaee Jordehi, A., Javadi, M.S., Catalão, J.P.S.: Optimal placement of battery swap stations in microgrids with micro pumped hydro storage systems, photovoltaic, wind and geothermal distributed generators. Int. J. Electr. Power Energy Syst. 125, 106483 (2021)
34. Jamian, J.J., et al.: Simulation study on optimal placement and sizing of battery switching station units using artificial bee colony algorithm. Int. J. Electr. Power Energy Syst. 55, 592–601 (2014)
35. Zheng, Y., et al.: The optimal configuration planning of energy hubs in urban integrated energy system using a two-layered optimization method. Int. J. Electr. Power Energy Syst. 123, 106257 (2020)
36. Zhang, X., et al.: Towards holistic charging management for urban electric taxi via a hybrid deployment of battery charging and swap stations. Renewable Energy 155, 703–716 (2020)
37. Liu, X.: Bi-level planning method of urban electric vehicle charging station considering multiple demand scenarios and multi-type charging piles. J. Energy Storage 48, 104012 (2022)
38. Zhang, H., Qiu, J., Wang, Y.: Planning strategy of fast-charging stations in coupled transportation and distribution systems considering human health impact. Int. J. Electr. Power Energy Syst. 133, 107316 (2021)
39. Wang, C., et al.: Active–reactive power approaches for optimal placement of charge stations in power systems. Int. J. Electr. Power Energy Syst. 84, 87–98 (2017)
40. Alhazmi, Y.A., Mostafa, H.A., Salama, M.M.A.: Optimal allocation for electric vehicle charging stations using trip success ratio. Int. J. Electr. Power Energy Syst. 91, 101–116 (2017)
41. Suresh, V., et al.: Optimal location of an electrical vehicle charging station in a local microgrid using an embedded hybrid optimizer. Int. J. Electr. Power Energy Syst. 131, 106979 (2021)
42. Javad Mirzaei, M., Siano, P.: Dynamic long-term expansion planning of electric vehicle parking lots considering lost opportunity cost and energy saving. Int. J. Electr. Power Energy Syst. 140, 108066 (2022)
43. Lin, X., et al.: Distribution network planning integrating charging stations of electric vehicle with V2G. Int. J. Electr. Power Energy Syst. 63, 507–512 (2014)
44. Abdi-Siab, M., Lesani, H.: Distribution expansion planning in the presence of plug-in electric vehicle: A bilevel optimization approach. Int. J. Electr. Power Energy Syst. 121, 106076 (2020)
45. Aluisio, B., et al.: Planning and reliability of DC microgrid configurations for Electric Vehicle Supply Infrastructure. Int. J. Electr. Power Energy Syst. 131, 107104 (2021)
46. Fan, V.H., Dong, Z., Meng, K.: Integrated distribution expansion planning considering stochastic renewable energy resources and electric vehicles. Appl. Energy 278, 115720 (2020)
47. Wang, S., et al.: Joint planning of active distribution networks considering renewable power uncertainty. Int. J. Electr. Power Energy Syst. 110, 696–704 (2019)
48. Li, X., et al.: Multi-year planning for the integration combining distributed energy system and electric vehicle in neighborhood based on data-driven model. Int. J. Electr. Power Energy Syst. 140, 108079 (2022)
49. Luo, L., et al.: Joint planning of distributed generation and electric vehicle charging stations considering real-time charging navigation. Appl. Energy 242, 1274–1284 (2019)
50. Hu, D., Zhang, J., Zhang, Q.: Optimization design of electric vehicle charging stations based on the forecasting data with service balance consideration. Appl. Soft Comput. 75, 215–226 (2019)
51. Luo, L., et al.: Optimal planning of electric vehicle charging stations comprising multi-types of charging facilities. Appl. Energy 226, 1087–1099 (2018)
52. Acharya, S., Dvorkin, Y., Pandzic, H., Karri, R.: Cybersecurity of smart electric vehicle charging: A power grid perspective. IEEE Access 8, 214434–214453. (2020)
53. Naderi, E., Asrari, A.: Integrated power and transportation systems targeted by false data injection cyberattacks in a smart distribution network. In: Electric Transportation Systems in Smart Power Grids, 'Integration, Aggregation, Ancillary Services, and Best Practices', 1st ed. pp. 447–472. CRC Taylor & Francis, Boca Raton, FL (2023)
54. Liang, G., Weller, S.R., Zhao, J., Luo, F., Dong, Z.Y.: The 2015 Ukraine blackout: Implications for false data injection attacks. IEEE Trans. Power Syst. 32(4), 3317–3318 (2017)

55. Li, E., Kang, C., Huang, D., Hu, M., Chang, F., He, L., Li, X.: Quantitative model of attacks on distribution automation systems based on CVSS and attack trees. Information 10(8), 251 (2019)
56. Eldewahi, A., Basheir, E.: Authenticated key agreement protocol for virtual private network based on certificateless cryptography. In: International Conference on Computing, Electrical, and Electronic Engineering (ICCEEE). Khartoum, Sudan, pp. 269–273 (2013)
57. Yari, I.A., Abdullahi, B., Adeshina, S.A.: Towards a framework of configuring and evaluating ModSecurity WAF on Tomcat and Apache web servers. In: International Conference on Electronics, Computer and Computation (ICECCO). Abuja, Nigeria, pp. 1–7 (2019)
58. He, C., Zhu, J., et al.: Optimal planning of electric vehicle battery centralized charging station based on EV load forecasting. IEEE Trans. Ind. Appl. 58(05), 6557–6575 (2022)
59. He, C., Zhu, J., et al.: Sizing and locating planning of EV centralized-battery-charging-station considering battery logistics system. IEEE Trans. Ind. Appl. 58(04), 5184–5197 (2022)
60. Shao, C., et al.: Coordinated planning of extreme fast charging stations and power distribution networks considering on-site storage. IEEE Trans. Intell. Transp. Syst. 22(1), 493–504 (2021)
61. Gan, W., et al.: Coordinated planning of transportation and electric power networks with the proliferation of electric vehicles. IEEE Trans. Smart Grid 11(5), 4005–4016 (2020)
62. Zeng, B., et al.: An optimal integrated planning method for supporting growing penetration of electric vehicles in distribution systems. Energy 126, 273–284 (2017)
63. Han, T., et al.: Load ratio optimization of urban power grid considering penetration of electric vehicles. In: 2018 IEEE 3rd Advanced Information Technology, Electronic and Automation Control Conference (IAEAC). Chongqing, China (2018)
64. Li, Y., et al.: Many-objective distribution network reconfiguration via deep reinforcement learning assisted optimization algorithm. IEEE Trans. Power Delivery 37, 2230–2244 (2022)

How to cite this article: He, C., Zhu, J., Borghetti, A., Liu, Y., Li, S.: Coordinated planning of charging swapping stations and active distribution network based on EV spatial-temporal load forecasting. IET Gener. Transm. Distrib. 1–21 (2023). https://doi.org/10.1049/gtd2.12915